The Significance of Dynamical Architecture for Adaptive Responses to Mechanical Loads During Rhythmic Behavior

Kendrick M. Shaw · **Miranda J. Cullins** · **Jeffrey M. McManus** · **Hui Lu** · **Peter J. Thomas** · **Hillel J. Chiel**

Abstract Many behaviors require reliably generating sequences of motor activity while adapting the activity to incoming sensory information. This process has often been conceptually explained as either fully dependent on sensory input (a chain reflex) or fully independent of sensory input (an idealized central pattern generator, or CPG), although the consensus of the field is that most neural pattern generators lie somewhere between these two extremes. Many mathematical models of neural pattern generators use limit cycles to generate the sequence of behavior, but other models, such as a heteroclinic channel (an attracting chain of saddle points), have been suggested. To explore the continuum between CPGs and chain reflexes, in this paper we describe a nominal model of feeding in *Aplysia californica* that can be smoothly shifted between a generic limit cycle (where the velocity changes by less than an order of magnitude throughout the cycle) and a heteroclinic channel (where the velocity becomes small when the trajectory passes near saddle points). We then study the behavior of the system in these two parameter regimes and compare the behavior of the models with behavior recorded in the animal *in vivo* and *in vitro*. We show that while both pattern generators can generate similar behavior, the stable heteroclinic channel can better respond to small changes in sensory input induced by load, and that the response matches the changes seen when a load is added *in vivo*. We then show that the stable heteroclinic channel shows much more dramatic slowing of activity than the generic limit cycle when sensory input is reduced, and show that similar slowing with removal of proprioception is seen *in vitro*. Finally, we show that the distributions of burst lengths seen *in vivo* are better matched by the distribution expected from a stable heteroclinic channel than that expected from a

Kendrick M. Shaw
Department of Biology and Medical Scientist Training Program, Case Western Reserve University, 10900 Euclid Ave., Cleveland OH 44106, USA
E-mail: kendrick.shaw@case.edu

Miranda J. Cullins · Jeffrey M. McManus · Hui Lu
Department of Biology, Case Western Reserve University, 10900 Euclid Ave., Cleveland OH 44106, USA

Peter J. Thomas
Departments of Mathematics, Biology and Cognitive Science, Case Western Reserve University, 10900 Euclid Ave., Cleveland OH 44106, USA
E-mail: peter.j.thomas@case.edu

Hillel J. Chiel
Departments of Biology, Neurosciences and Biomedical Engineering, Case Western Reserve University, 10900 Euclid Ave., Cleveland OH 44106, USA
E-mail: hjc@case.edu

generic limit cycle. These observations suggest that feeding behavior in *Aplysia* may be better described by a model using a heteroclinic channel than a more generic limit cycle.

Keywords Aplysia · heteroclinic channel · Central Pattern Generator · Chain reflex · Limit cycle

1 Introduction

Motor behaviors, such as cat running, crayfish swimming, and dog lapping all require the nervous system to reliably generate a sequence of motor outputs. To be efficient, however, a fixed sequence of activity is not enough: a cat that fails to step over an obstacle may lose its footing and fall (Forssberg et al, 1975; Forssberg, 1979) and a crayfish that wanders into a current of cold water must control muscles that may suddenly have become stronger but relax more slowly (Harri and Florey, 1977). Sensory feedback plays a key role in allowing an animal to adapt its behavioral pattern to the circumstances in which it finds itself. The way that this sensory information is integrated into pattern generation to produce adaptive behavior, however, can be difficult to ascertain.

Historically, two competing theories have been proposed for how the nervous system can generate sequences of motor activity (Marder and Bucher, 2001). At one extreme, Loeb (1899) proposed that sensory input is required for the transitions between behaviors, so that the sequence of behavior is formed of a chain of reflexes each leading to the next. He thus proposed calling this form of pattern generation a "kettenreflex," or "chain reflex." For example, during walking, this theory would predict that extension of the leg continues until sensory input indicates that the foot has struck the ground, and in the absence of this sensory input, the pattern would not progress. This theory was later elaborated by Sherrington, who noted that bouts of walking-like movements could be evoked in the hind limbs of a dog after spinal transection by dropping the limb, and these motor patterns would stop abruptly when the limb was passively mechanically arrested (Sherrington, 1910).

Even chain reflex theory's strongest advocates saw it as an incomplete explanation of what was observed in the biology, however. Sherrington, noting that spinal stimulation could produce step-like movements even in a deafferented limb, concluded "These difficulties suggest that generation of a secondary local stimulus and its interference with the operation of the primary remote stimulus, although regulative of the rhythm (cf. vagus and respiratory rhythm) is of itself not the sole rhythm-producing factor in the reflex." By the time Wilson showed that the nervous system in the locust could generate strong structured motor patterns in the absence of sensory input (Wilson, 1961), investigators had come to assume that sequences of motor activity were primarily generated by a central pattern generator. The central pattern generator theory suggests that the nervous system can, on its own, produce appropriate patterns of motor activity even in the absence of sensory input. At best, sensory input merely serves to modulate this underlying neural pattern.

It should be noted, however, that patterns generated by the isolated nervous system often are very distorted compared to those seen *in vivo*. In particular, phases of the motor pattern are often significantly longer than those observed in the intact animal. This has led many investigators to question the descriptive power of central pattern generator theory. In the words of Robertson and Pearson, "Although now abundantly clear that a central rhythm generator can produce powerful oscillations in the activity of flight motor neurons and interneurons, it is equally clear that the properties of this central oscillator cannot fully account for the normal flight pattern" (Selverston, 1985).

There is some evidence that slowing of isolated neural patterns may be due to the absence of sensory feedback. In Pearson et al (1983), cycle-by-cycle stimulation of the appropriate sensory afferents was able to restore wing-beat frequency in fictive flight in the locust. Restoration of the normal pattern by sensory input suggests that biological pattern generators may occupy a middle ground between pure central pattern generators and chain reflexes. In some

cases, endogenous neural input may control where a systems lies on this continuum. As Bässler (1986) noted when considering a relaxation-oscillator like model of a central pattern generator "Hence, one and the same system can behave either like a CPG or like a chain reflex, depending only on the amount of endogenous input." These investigators thus warned about the dangers of inferring the mechanism used by a pattern generator *in vivo* based only on the behavior of a pattern generator *in vitro*.

Despite these hesitations, the empirical data supporting central pattern generator hypothesis led to a focus on providing a mathematical formulation for this theory using the qualitative analysis of dynamical systems, which was becoming an important tool for theoretical neuroscience by the middle of the twentieth century. The behavior of an ideal central pattern generator naturally corresponds to a system of nonlinear ordinary differential equations whose solutions contain stable limit cycle (an attracting isolated periodic orbit). As a result, this structure has played a central role in the mathematical description of central pattern generators (Ijspeert, 2008).

In contrast, there have been fewer attempts to model chain reflexes with systems of differential equations. Instead, much of the work modeling these types of sensory-dependent systems use different tools, such as finite state machines (Lewinger et al, 2006). While these models can capture individual phases of the behavior well, they generally do not describe the transitions between the phases, which may be important in understanding some forms of behavior. In contrast, one could view the state of a chain reflex system in terms of a series of stable fixed points. In each phase of the motion, the trajectory would be captured by one of the fixed points until the appropriate (external) sensory input pushed the system out of the neighborhood attracted to that fixed point and into the basin of attraction of the next.

Between these two extremes of models of central pattern generators and chain reflexes, one may consider systems in which the progress of a periodic orbit is slowed, but not stopped, by passage near one or more fixed points. This behavior arises naturally in a structure known as a "stable heteroclinic channel" (Rabinovich et al, 2008), where multiple saddle points (fixed points that attract in some directions while repelling in others) are connected in a cycle, so that the unstable manifold of each saddle point brings the system near the stable manifold of the next fixed point. This structure has been used to describe motor behavior such a predatory swimming behavior in *Clione* (Levi et al, 2004; Varona et al, 2004). To our knowledge, however, these models of pattern generation have not been directly compared to those built with a more "pure" limit cycle that does not pass near fixed points.

A potential advantage of a dynamical system that allows trajectories to move close to equilibrium points is that it may spend longer or shorter times in that vicinity, rather than proceeding through the cycle with a relatively fixed phase velocity. In turn, this could allow an animal greater flexibility in responding to unexpected changes in the environment, such as increases or decreases in mechanical load as it attempts to manipulate an object.

To examine this range of dynamics, we have created a neuromechanical model based on the feeding apparatus of the marine mollusk *Aplysia californica*. We examine the model in two parameter regimes which produce similar output under small loads. In the first parameter regime, the isolated neural dynamics form a homogeneous limit cycle, as would be expected for an idealized central pattern generator. In the second parameter regime, the isolated neural dynamics form a stable heteroclinic cycle, moving it closer along the continuum to a chain reflex. We show that in this second regime, the behavior of the model falls between that of an idealized chain reflex and an idealized central pattern generator. We then compare the behavior of the two models to the observed behavior of the animal, and show that several of the features of the animal's behavior are better described by the model with the stable heteroclinic channel than the model with the limit cycle. At the end of the paper, we reflect on possible general principles suggested by this work.

2 Mathematical Framework

In this section we describe a general mathematical framework we will use for modeling the behavior of motor pattern generators. We model a central pattern generator receiving sensory input from the body as a system of differential equations specifying the evolution of a vector of n neural state variables, $a \in \mathbb{R}^n$, and a vector of m state variables, $x \in \mathbb{R}^m$, representing the mechanics and periphery (e.g. muscle activation). We assume that an applied load interacts only with the mechanical state variables, so that the differential equations can be naturally written in the following form:

$$\frac{da}{dt} = f(a, \mu) + \varepsilon g(a, x), \tag{1}$$

$$\frac{dx}{dt} = h(a, x) + \kappa l(x). \tag{2}$$

Here μ is a vector of parameters which can encode states such as arousal of the animal, $f(a, \mu)$ represents the intrinsic dynamics of a motor pattern pattern generator, $h(a, x)$ represent the dynamics of the periphery with the given central input, $g(a, x)$ represents the effects of sensory feedback from the periphery, $l(x)$ represents the effects of an external load or perturbation, and $\varepsilon, \kappa \in \mathbb{R}^+$ are scaling constants, not necessarily small. We further assume that all of these functions are smooth, infinitely differentiable, and have bounded ranges over the domain of interest.

2.1 Limit cycles

We first consider the case of an idealized central pattern generator, where a part of the nervous system can produce sequences of motor activity that closely resemble those seen *in vivo*, even when it is not attached to the periphery. Thus we assume that, for some range of the parameter μ, the dynamics of the isolated neural circuit, $da/dt = f(a, \mu)$, contain an attracting limit cycle $\gamma(t)$ which represents the observed motor pattern. We make the further important assumption that there exists a behaviorally relevant

mechanical load $\kappa l(x)$ with which the complete system contains a corresponding limit cycle $\xi(t)$, such that the neural component of $\xi(t)$ closely matches that of the isolated system. By this we mean that, with appropriately chosen initial conditions,

$$\int_0^T ||\gamma(t) - P_a \xi(t)||^2 \, dt \ll 1, \tag{3}$$

where $P_a : \mathbb{R}^{m+n} \to \mathbb{R}^n$ is the projection operator onto the a subspace, T is the period of $\gamma(t)$, and $|| \cdot ||$ is the usual L^2 (Euclidean) norm. Note that it is possible that these very similar patterns will produce very different behavior in the periphery. Therefore, we will also assume that this isolated pattern $\gamma(t)$ produces similar behavior in the periphery, that is that the system $dx/dt = h(\gamma(t), x) + \kappa l(x)$ contains an attracting periodic orbit $\zeta(t)$ such that with an appropriate choice of initial conditions

$$\int_0^T ||\zeta(t) - P_x \xi(t)||^2 \, dt \ll 1, \tag{4}$$

where $P_x : \mathbb{R}^{m+n} \to \mathbb{R}^m$ is the projection operator onto the x subspace. Finally, we assume that gradually adding back sensory input does not distort the pattern or the behavior, meaning that both $\gamma(t)$ and $\zeta(t)$ persist for small values of ε and remain similar to projections of $\xi(t)$.

Because the system is smooth, the integral in (3) can be made to be small by insuring that the magnitude of the sensory feedback, $||\varepsilon g(P_a \xi(t), P_x \xi(t))||$, is small for all $t \in (0, T)$. Although a careful choice of $||g||$ could be small along ξ but not elsewhere, we will focus on the more generic case where $\varepsilon \ll 1$.

2.2 Destabilization of fixed points

We next consider the chain reflex. In this case the dynamics of the isolated nervous system, $da/dt = f(a, \mu)$, will contain a set of stable nodes, A, where each node represents a "stage" of the chain reflex, that can be destabilized by sensory input. Note that in this case, unlike the central pattern generator, ε may need to be of $O(1)$ to destabilize a node. The combined dynamics of the nervous system and the

periphery, however, would still be expected to contain a stable limit cycle $\xi(t)$ rather than a series of fixed points. Similar dynamics have been seen in models of other biological oscillators; for example in Novak et al (1998) the authors created a model of the cell cycle where fixed points in the biochemical dynamics (analogous to the isolated neural dynamics) can be destabilized by changes in cell size (analogous to the periphery) so that the coupled system contains a limit cycle. Because a chain reflex can not explain the fictive motor patterns produced by the isolated nervous system, we will not explore this alternative in in this paper.

2.3 Stable heteroclinic channels

We now consider a system that is intermediate between the two extremes of an idealized central pattern generator and a chain reflex. We can construct such a system from a set of n-dimensional hyperbolic saddle points, each with a one-dimensional unstable manifold and an $n-1$ dimensional stable manifold, arranged in a cycle such that the unstable manifold of one saddle point intersects the stable manifold of the next, forming a heteroclinic orbit. We refer to these saddle points and their connecting heteroclinic orbits as a *heteroclinic cycle* (Guckenheimer and Holmes, 1988).

Under appropriate conditions, this heteroclinic cycle attracts nearby orbits (and thus can be called a stable heteroclinic cycle). In particular, if we define the (positive) ratio of the least negative stable eigenvalue $\lambda_{i,\mathrm{s}}$ and the unstable eigenvalue $\lambda_{i,\mathrm{u}}$ of the ith saddle as the saddle index $v_i = -\lambda_{i,\mathrm{s}}/\lambda_{i,\mathrm{u}}$ (Shilnikov et al, 2002), then the heteroclinic cycle will attract nearby orbits if $\prod_i v_i > 1$ (**?**). This type of dynamics can arise naturally from neural models involving symmetric mutually inhibitory pools of neurons; for example see Nowotny and Rabinovich (2007).

An unperturbed trajectory on the heteroclinic cycle will, like the chain reflex model in section 2.2, asymptotically approach a fixed point. Unlike the chain reflex model, however, a very small perturbation in the unstable direction will push the trajectory out of the stable manifold, allowing the trajectory to leave the neighborhood of the fixed point (and potentially travel to the neighborhood of the next fixed point). Arbitrarily small amounts of noise can thus insure that the system will almost certainly not remain stuck at a given fixed point (Stone and Holmes, 1990). Thus, rather than the stability of states seen in the chain reflex model, the heteroclinic cycle exhibits metastability (Afraimovich et al, 2011), where the trajectory spends long but finite periods of time near each fixed point (Bakhtin, 2011). Thus, like the chain reflex, the system can spend short or long periods of time in one particular state depending on sensory input, but, like the limit cycle, the system will eventually transition to the next state even in the absence of sensory input.

While stable heteroclinic cycles are structurally unstable (i.e. a small change in the vector field will generally break the cycle), small perturbations can result in the creation of a stable limit cycle that passes very close to the saddles. For example, in the planar case, any sufficiently small perturbation that pushes the unstable manifold of the saddles towards the inside of the unperturbed stable heteroclinic cycle will result in a stable limit cycle (Reyn, 1980). Similar conditions can be found for higher dimensional stable heteroclinic cycles (**?**). These families of limit cycles that pass close to the original saddles, known as stable heteroclinic channels (Rabinovich et al, 2008), are structurally stable, and exhibit many of the same properties of sensitivity and metastability as the original stable heteroclinic cycles. As we will see, this extreme sensitivity can be advantageous for generating adaptive behaviors.

In the next section we provide an example of model dynamics $f(a,\mu)$ exhibiting a limit cycle for $\mu > 0$ and a bifurcation to a heteroclinic cycle at $\mu = 0$. We then investigate the behavior of the full (a,x) system in the "limit cycle" and "heteroclinic cycle" parameter regimes.

3 Model Description

3.1 Neural model

We wish to explore the effects of different types of neural dynamics on the behavior of the animal. Although detailed, multi-cellular and multi-conductance models of neurons and circuits underlying feeding pattern generation in *Aplysia* have been described (Baxter and Byrne, 2006; Cataldo et al, 2006; Susswein et al, 2002), the complexity of these models makes it difficult to use them for mathematical analysis. As a consequence, we choose to represent motor pools (which contain neurons that are electrically coupled to one another or have mutual synaptic excitation) using nominal firing-rate models.

As discussed in section 2, we define the neural dynamics as a combination of an intrinsic component, $f(a,\mu)$, that does not depend on the periphery, and a sensory (coupling) component, $g(x)$, which does depend on the periphery. For mathematical tractability, we assume that the intrinsic and sensory drive combine linearly, thus giving the evolution equation of the neural activity.

$$\frac{da}{dt} = f(a,\mu) + \varepsilon g(x_{\mathrm{r}}), \tag{5}$$

where a is a vector of the activity of each of the N neurons, ε is a parameter scaling the strength of sensory input, x_{r} is a biomechanical state variable which we will define in more detail in section 3.2, and μ is a parameter that can shape the intrinsic dynamics. Specifically we will consider the following modified Lotka–Volterra model which captures the dynamics of N neural pools:

$$f_i(a,\mu) = \frac{1}{\tau_{\mathrm{n}}} \left(\left(1 - \sum_j \rho_{ij} a_j \right) a_i + \mu \right), \tag{6}$$

for $0 \le i < N$. Here μ is a scalar parameter representing intrinsic excitation, τ_{n} is a time constant, and ρ is the coupling matrix

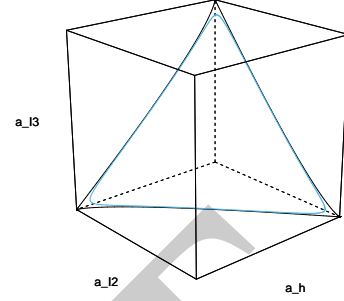$$\rho_{ij} = \begin{cases} 1 & i = j \\ 0 & i = j-1 \pmod{N} \\ \gamma & \text{otherwise,} \end{cases} \tag{7}$$

Fig. 1: When $\mu = 0$, in the absence of sensory input ($\varepsilon = 0$), the intrinsic neural dynamics contain a stable heteroclinic cycle (black line) connecting saddles at $(1,0,0)$, $(0,1,0)$, and $(0,0,1)$. When μ is a small positive number and $\varepsilon = 0$, the heteroclinic cycle is broken and a stable limit cycle arises (shown in light blue for the value of μ used for the limit cycle in this paper).

where γ is a coupling constant representing inhibition between neural pools.

When $N > 2$ and $\gamma > 2$ this system contains a stable heteroclinic cycle when $\mu = 0$. In contrast, as shown in figure 1, it contains a stable limit cycle for small positive values of μ, with the distance between the limit cycle and saddles increasing with increasing values of μ. With the goal of parsimony, we use $N = 3$ and thus (6) can be expanded to

$$f_0(a,\mu) = \frac{1}{\tau_{\mathrm{n}}} (a_0(1 - a_0 - \gamma a_1) + \mu), \tag{8}$$

$$f_1(a,\mu) = \frac{1}{\tau_{\mathrm{n}}} (a_1(1 - a_1 - \gamma a_2) + \mu), \tag{9}$$

$$f_2(a,\mu) = \frac{1}{\tau_{\mathrm{n}}} (a_2(1 - a_2 - \gamma a_0) + \mu). \tag{10}$$

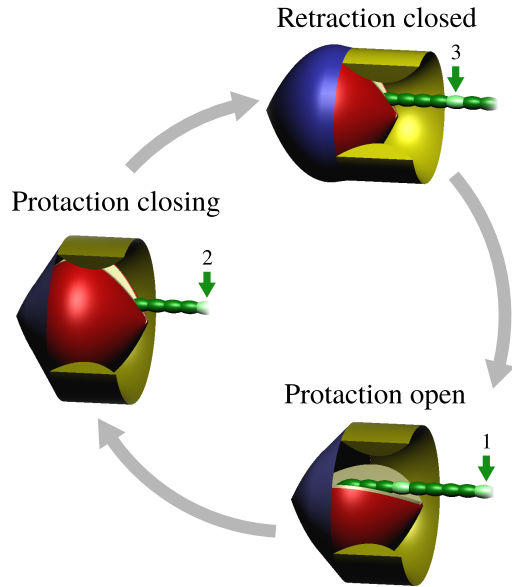We explain the correspondence of these three neural pools to neural pools in *Aplysia* in the next section.

Fig. 2: The model breaks swallowing into three phases. First, the odontophore protracts while open (lower right). Near the end of protraction, the odontophore begins closing (left) and protracts a small distance while closed. In the last phase, the odontophore retracts while closed (upper right). The protraction muscle (I2) is shown in blue, the grasper (the radula-odontophore) is shown in red, and the ring-like retraction muscle (I3) is shown in yellow, with a section cut away to show the grasper. The green strand is seaweed, with the arrows showing how the seaweed moves within a single cycle.

Fig. 3: Schematic of the neuromechanical model of the feeding apparatus in *Aplysia*. The three neural pools (a_0, a_1, and a_2) control three phases of the behavior shown in figure 2: protraction open, protraction closing, and retraction closed. The solid lines and triangles indicate excitatory synaptic coupling with a neuromuscular transform represented by a low pass filter. The dashed line and summation symbol represent a simple summation and thresholding that control closing in the model. The a_0 neural pool represents the B31, B32, and B63 neurons, the a_1 motor pool represents these same neurons with the addition of B8 (which experiences slow excitation from B34), and the a_2 motor pool represents B64, B3, B6, B9, and B8 (which is excited by B64) activity.

3.2 Model of the periphery and load

We next couple the neural dynamics to a nominal mechanical model of feeding in *Aplysia*. During ingestive behaviors in *Aplysia*, a grasper, known as the radula-odontophore, is protracted through the jaws by a muscle referred to as I2. The grasper closes on food, and then is retracted by a muscle called I3, and then opens again, completing the cycle (see figure 2). The timing of closing is often not precisely align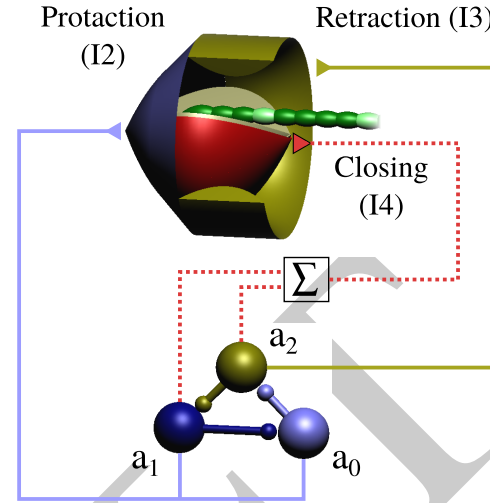ed with the switch from protraction to retrac- tion. Instead, closing usually occurs before the end of protraction, although the amount of overlap varies by behavior, from very little overlap in swallows to a significant overlap in rejection. A general model for biting and swallowing could thus contain four components - protraction while open, protraction while closed, retraction while closed, and retraction while open. For simplicity, we reduce these to three components, each of which corresponds to one of the three

parameter	value	description
γ	2.4	inhibition strength from next pool
ε	$2 \cdot 10^{-3}$	sensory feedback strength
κ	$3\sqrt{3}/2$	length-tension curve normalization constant
μ	0	neural pool intrinsic excitation
σ_0	-1	proprioceptive direction for protraction open neural pool
σ_1	1	proprioceptive direction for protraction closing neural pool
σ_2	1	proprioceptive direction for retraction closed neural pool
τ_n	0.05	neural pool time constant
τ_m	0.05	muscle activation time constant
b_r	0.10	grasper damping constant
b_{sw}	0.10	seaweed damping constant
c_0	1	position of shortest length for I2
c_1	1.1	position of center of I3
F_{sw}	0.01	force on the seaweed resisting ingestion
k_0	-1	I2 muscle strength and direction
k_1	1	I3 muscle strength and direction
S_0	0.5	proprioceptive neutral position for protraction open neural pool
S_1	0.5	proprioceptive neutral position for protraction closing neural pool
S_2	0.25	proprioceptive neutral position for retraction closed neural pool
u_{max}	1	maximum muscle activation
w_0	2	maximal effective length of I2
w_1	1.1	maximal effective length of I3

Table 1: Model parameters

state variable	initial value	description
a_0	1.0	activity of I2 motor pool (non-negative)
a_1	10^{-9}	activity of hinge motor pool (non-negative)
a_2	10^{-9}	activity of I3 motor pool (non-negative)
u_0	0.0	activity of I2 muscle
u_1	0.0	activity of I3 muscle
x_r	0.5	grasper position (0 is retracted, 1 is protracted)
x_{sw}	0.0	seaweed position (positive is away from the animal)

Table 2: State variables

these same I2 motor neurons with the addition of the B8 motor neurons, which activate the I4 muscle used in closing(Morton and Chiel, 1993). The retraction closed pool (a_2) contains B8 with the addition of the I3 motor neurons B3, B6, and B9 which are simultaneously active during retraction (Church and Lloyd, 1994). Thus the I2 muscle will be driven by both protraction-open (a_0) and protraction-closing (a_1) motor pools, whereas the I3 muscle is driven by a single motor pool (a_2).

The I2 and I3 muscles are known to respond slowly to neural inputs (Yu et al, 1999); we thus model their activation as a low-pass filter of the neural inputs using the time constants from the model of the I2 muscle described by Yu et al (1999). Using u_i for the activation of the ith muscle, τ_m for the filter's time constant, we use

$$\frac{du_0}{dt} = \frac{1}{\tau_m}((a_0 + a_1)u_{max} - u_0), \tag{11}$$

$$\frac{du_1}{dt} = \frac{1}{\tau_m}(a_2 u_{max} - u_1). \tag{12}$$

In general, the force a muscle can exert will vary with the length to which it is extended (Zajac, 1989; Fox and Lloyd, 1997). The shape of this curve is typically explained by the sliding filament theory as follows: for some maximal length, the actin and myosin fibers will not overlap and the muscle will be limited to passive forces, but below that length, the force will first rise with the increasing overlap of the

neural pools in the neural model: protraction open, protraction closing, and retraction open, as shown in figure 3. The protraction open motor pool (a_0) corresponds to the electrically coupled group of neurons B31, B32, B61, B62, and B63, which activate the I2 muscle and are all active during protraction (Hurwitz et al, 1996, 1997; Susswein et al, 2002). The protraction closing neuron pool (a_1) corresponds to

actin and myosin fibers, reach a maximum, and then decline as the overlapping fibers start to exert steric effects (Gordon et al, 1966). More recently, changes in lattice spacing between the fibers has also been shown to have a role in the force-length dependence (Williams et al, 2013). We model this length/tension curve using the following simple cubic polynomial:

$$\phi(x) = -\kappa x(x-1)(x+1) \tag{13}$$

where κ is a scaling constant. This equation crosses through zero force at zero length and again reaches zero at the nominal maximal length of 1. We let $\kappa = 3\sqrt{3}/2$ to normalize the maximum force between these two points to 1 (which occurs at a length of $1/\sqrt{3}$).

Although mechanical advantage plays an important role in swallowing (Sutton et al, 2004b; Novakovic et al, 2006), when combined with the length tension curve, the resulting force resembles a shifted and rescaled version of the original length tension curve over the range of motion used in swallowing. We thus choose position and scaling constants for the length-tension curve to approximate the resultant force curve in the biomechanics, rather than the length-tension curve of the isolated muscle.

We assume the tension on each muscle is linearly proportional to its activation, and sum all of the muscle forces giving

$$F_{\text{musc}} = \sum_i k_i \phi\left(\frac{x_r - c_i}{w_i}\right) u_i. \tag{14}$$

Here $x_r \in (0, 1)$ is the position of the grasper, k_i is a parameter representing the strength and direction of each muscle, c_i the position of the grasper where the ith muscle is at its minimum effective length, and w_i the difference between the maximum and minimum effective lengths for the ith muscle. The sign of k_i determines the direction of force of the muscle; when k_i is negative (as it is for I2) the muscle will pull towards its position of shortest length, and when it is positive (as it is for I3) it will push away from this position (in the case of I3, squeezing the radula-odontophore out of the ring of the jaws.

We model opening and closing of the odontophore (and thus holding and releasing the seaweed) as a simple binary function, where the odontophore is closed when certain motor pools are active and open otherwise. Specifically, the radula was considered to be closed when $a_1 + a_2 \geq 0.5$, and open when $a_1 + a_2 < 0.5$. This threshold can be viewed as a plane dividing phase space into two regions with different mechanics (holding the seaweed and not holding the seaweed).

In our experience, the teeth on the radula tend to hold the seaweed very firmly, and the animal tends to let go before the seaweed slips from its grasp. Thus the seaweed and the odontophore are considered to be "locked together" when the odontophore is closed and we do not attempt to model slip. The seaweed is assumed to be pulling back with a constant force F_{sw}, which is included in the net force on the odontophore when the odontophore is closed

The seaweed and odontophore are assigned viscous damping constants b_{sw} and b_r, respectively; thus the full equations of motion are

$$\frac{dx_r}{dt} = v_r \tag{15}$$

$$\frac{dx_{\text{sw}}}{dt} = v_{\text{sw}} \tag{16}$$

$$\frac{dv_r}{dt} = \frac{F_{\text{musc}} - b_r v_r}{m_r} \tag{17}$$

$$\frac{dv_{\text{sw}}}{dt} = \frac{F_{\text{sw}} - b_{\text{sw}} v_{\text{sw}}}{m_{\text{sw}}} \tag{18}$$

when the odontophore is open, and

$$\frac{dx_r}{dt} = \frac{dx_{\text{sw}}}{dt} = v_r \tag{19}$$

$$\frac{dv_r}{dt} = \frac{F_{\text{musc}} + F_{\text{sw}} - (b_r + b_{\text{sw}})v_r}{m_r + m_{\text{sw}}} \tag{20}$$

$$v_{\text{sw}} = v_r \tag{21}$$

when the odontophore is closed. Note that that we are assuming that the momentum of the seaweed is negligible.

We have observed that when seaweed is abruptly pulled, animals respond with rapid movements of the radula/odontophore without oscillations. This suggests that the system is at least critically damped

under these conditions, if not over damped. Furthermore, since the mass of the buccal mass is very small (a few grams), and the accelerations during movement are typically small (based on MRI measurements, they may be close to zero during most of the motion (Neustadter et al, 2002, 2007)), we choose to use equations of motion that assume a viscous limit. Thus, instead of directly simulating equations 15-21, we use the following reduced system:

$$\frac{dx_r}{dt} = \frac{F_{musc}}{b_r} \qquad (22)$$

$$\frac{dx_{sw}}{dt} = \frac{F_{sw}}{b_{sw}} \qquad (23)$$

when the odontophore is open, and

$$\frac{dx_{sw}}{dt} = \frac{dx_r}{dt} = \frac{F_{musc} + F_{sw}}{b_r + b_{sw}} \qquad (24)$$

when the odontophore is closed. For simulations without a mechanical load, where $F_{sw} = 0$ and $b_{sw} = 0$, we replace this equation with

$$\frac{dx_{sw}}{dt} = 0, \qquad (25)$$

which leaves the seaweed stationary when the radula-odontophore is open.

It is entirely possible that the system is effectively quasi-static, and that positional forces dominate over viscous forces, but this formulation does not assume that from the outset.

In some of the simulations we wish to simulate seaweed that is held or fixed in place rather than experiencing a constant force. For these simulations we replace the constant F_{sw}, with a function modeling the force as a stiff spring using Hooke's law, i.e.

$$F_{sw}(x_{sw}) = (x_{spring} - x_r)k_{spring}. \qquad (26)$$

3.3 Proprioceptive input

Proprioceptive neurons detect the position of and forces within the animal's body. These mechanoreceptors can take many forms, from the muscle spindles and golgi tendon organs of vertebrates to the muscle organs seen in crustaceans to the S-channel expressing neurons seen in mollusks(Vandorpe et al, 1994). Rather than model these in detail, we have assumed that, as a function of the position of the grasper, the proprioceptive sensory neurons will create a net excitation or inhibition of each neural pool. For simplicity we have used a linear relation for this proprioceptive input as a function of position,

$$g(x_r) = (x_r - S_i)\sigma_i, \qquad (27)$$

where $x_r \in (0, 1)$ is the position of the grasper, S_i is the position where the net proprioceptive input to the ith neural pool is zero, and $\sigma_i \in \{-1, 1\}$ is the direction of proprioceptive feedback for the ith motor pool.

3.4 Noise

All biological systems are subject to noise, and as we will show, this can have important effects on the dynamics. Typical examples of noise in a neural context would include the small fluctuations caused by opening and closing of ion channels (known as channel noise (White et al, 2000; Goldwyn and Shea-Brown, 2011)), the variable release of neural transmitter vesicles, and stochastic effects from small numbers of molecules in second messenger systems. One can also treat parts of the system that we are not including in the model as "noise" (Schiff, 2012), such as small variations in sensory input from the environment with a mean of zero.

We model this noise as a 3-dimensional Weiner process of magnitude η (i.e. white noise). This form of noise arises naturally when the noise is created by many small identical independent events with finite variance, such as channels opening and closing. Although most biological noise is bandwidth limited, the higher frequencies of the noise are filtered out by the dynamics of the model and can thus be ignored. Noise is added to the neural state variables a_i, but assumed to be negligible for the mechanical state variable x_r. For simulations in which noise is used, we thus replace the ordinary differential equation (5)

parameter	value	description
β	0.20405	neural pool global time constant
μ	$1 \cdot 10^{-3}$	neural pool intrinsic excitation
α_0	0.6101	neural pool local time scaling near protraction open
α_1	-0.9201	neural pool local time scaling near protraction closing
α_2	0.276	neural pool local time scaling near retraction closed
$u_{\max}$	2.9	maximum muscle activation

Table 3: Parameters used for the limit cycle simulations

with the stochastic differential equation

$$da = \big(f(a,\mu) + \varepsilon g(x_{\mathrm{r}})\big)\,dt + \eta\,dW_t, \tag{28}$$

where W_t is a three-dimensional Weiner process.

3.5 Parameter changes used for the limit cycle simulations

As mentioned in section 3.1, the isolated neural dynamics (i.e. when $\varepsilon = 0$) exhibits a stable heteroclinic cycle when $\mu = 0$, and a stable limit cycle for small positive values of μ[1]. In this paper, we will be exploring the effects of these two different dynamical regimes on the ingestive behavior of the model. We will refer to them as the stable heteroclinic channel (where μ is zero) and the limit cycle (where $\mu > 0$). Note that when the neural dynamics is coupled to the dynamics of the periphery, for both models the combined system exhibits a stable limit cycle. For the remainder of the paper, however, we will use the phrase "the limit cycle" to refer to the model whose isolated neural dynamics exhibit a limit cycle, and "the stable heteroclinic channel" to refer

[1] For sufficiently large values of μ, the intrinsic excitation overwhelms the mutual inhibition between the pools and all of the pools become tonically active via a supercritical Hopf bifurcation. This tonic activity does not produce ingestive behavior in our model, so we will not examine it further in this paper.

to the model whose isolated neural dynamics exhibit a stable heteroclinic channel.

As we will describe in section 5.1, without additional tuning of the parameters, the limit cycle performs much more poorly than the stable heteroclinic channel. For the limit cycle models, we thus change a small number of parameters as shown in table 3. We also perform a phase dependent adjustment of timing by replacing the neural time constant τ_{n} with the following activity-dependent time scaling function

$$\tau_{\mathrm{n}}(a) = (1 + \alpha \cdot a)\beta. \tag{29}$$

Here β is a scalar parameter representing a uniform adjustment in the speed of the trajectories (analogous to the previous constant τ_{n}), and α is a vector parameter representing an activity-dependent scaling of the speed. Note that this change affects the timing but not the location of the trajectories in space in the isolated neural dynamics.

3.6 Connection to mathematical framework

This system can be understood within the mathematical framework presented in section 2. In particular, the neural state vector a, the neural dynamics f, and the sensory feedback g correspond to the variables and functions of the same name in (1). In the case of the full dynamics (15-21), the peripheral state vector x can be seen as the concatenation of u, x_{r}, and v_{r}. If we assume the mass of the seaweed to be negligible compared to the mass of the odontophore, we can then model l as a vector function with all components equal to 0 except for the v_{r} component of l when the odontophore is closed. We set this component equal to the change in force with the addition of the seaweed, i.e.

$$l_{v_{\mathrm{r}}} = \frac{F_{\mathrm{sw}} - b_{\mathrm{sw}}v_{\mathrm{r}}}{m_{\mathrm{r}}}. \tag{30}$$

4 Materials and Methods

Predictions of the model were tested using data from intact animals, from animals in which all but feed-

ing proprioceptive input had been removed (the suspended buccal mass), and preparations from which all sensory input had been removed (the isolated cerebral and buccal ganglia). Adult *Aplysia californica* were obtained from Marinus Scientific, Long-Beach CA, USA. The animals were housed in aerated 50 gallon aquariums at 16°C with a 12 hour light/dark cycle, and fed 0.5 g of dried laver every other day. Animals were presented with seaweed to test feeding behavior before use, and all animals used generated bites at 3 to 5 second intervals when tested.

4.1 Intact animals

Details of the recording methods for intact animals are described in Cullins and Chiel (2010). Briefly, animals from 350 g to 450 g were anesthetized by injecting 30% of the animal's mass of isotonic (0.333 molar) magnesium chloride solution into the hemocoel. Hook electrodes were then surgically implanted and attached to the I2 muscle, the radular nerve (RN), buccal nerve 2 (BN2), and buccal nerve 3 (BN3). The animals were allowed to recover, and then presented with 5 mm seaweed strips to elicit swallowing patterns. Video and EMG/ENG were recorded simultaneously to capture the behavior corresponding to the feeding motor patterns. Electrical recordings were made using an A-M Systems model 1700 amplifier with a 10-1000 Hz band-pass filter for EMG and a 100-1000 Hz bandpass filter for the ENG recordings, and captured using a Digidata 1300 digitizer and AxoScope software (Molecular Devices).

4.2 Suspended buccal mass preparation

The methods used for the suspended buccal mass are described in McManus et al (2012). Briefly, animals from 250 g to 350 g in weight were anesthetized by injecting 50% of the animal's mass of isotonic magnesium chloride into the hemocoel. The buccal mass and attached buccal and cerebral ganglia were then dissected out and placed in *Aplysia* saline (460 mM NaCl, 10 mM KCl, 22 mM MgCl$_2$, 33

mM MgSO$_4$, 10 mM CaCl$_2$, 10 mM glucose, 10 mM MOPS, pH 7.4–7.5). Hook electrodes were attached to the I2 muscle, RN, BN2, BN3, and branch a of BN2 (BN2a). The buccal mass was then suspended via sutures through the soft tissue at the rostral edge and the two ganglia pinned out behind it, with the cerebral ganglia placed in a separate chamber isolated from the main chamber using vacuum grease. To elicit ingestive patterns, the *Aplysia* saline in the chamber containing the cerebral ganglion was changed to a solution of 10 mM carbachol (Acros Organics) in *Aplysia* saline. Electrical recordings were made using an A-M Systems model 1700 amplifier with a 10-500 Hz band-pass filter for EMG and a 300-500 Hz bandpass filter for the ENG recordings, and captured using a Digidata 1300 digitizer and AxoGraph software (Axon Instruments).

4.3 Isolated buccal ganglion

The methods used for the isolated ganglia are described in Lu et al (2013). Briefly, the animal was euthanized and the buccal mass and buccal and cerebral ganglia dissected out as described for the suspended buccal mass. The ganglia were then dissected away from the buccal mass along with a small strip of I2 attached to the I2 nerve, and the ganglia was pinned out in a two-chambered dish lined with Sylgard 184 (Dow Corning), with a vacuum grease seal separating the solution in the chamber with the cerebral ganglion from that in the chamber with the buccal ganglion. Suction electrodes were attached to BN2, BN3, RN, and the excised strip of the I2 muscle. For ingestive patterns, a 10 mM carbachol solution was applied to the chamber containing the cerebral ganglion. Electrical recordings were made using an A-M Systems model 1700 amplifier with a 10-500 Hz band-pass filter for EMG and a 300-500 Hz bandpass filter for the ENG recordings, and captured using a Digidata 1300 digitizer and AxoGraph software (Axon Instruments).

4.4 Data analysis

Selection of patterns for analysis varied by preparation. For the intact animal, patterns were considered swallows if the video showed the animal grasping the seaweed throughout the pattern and the net movement of the seaweed was inward; other behaviors such as bites and rejections were not studied for this paper. For the suspended buccal mass and isolated ganglia, patterns were used near the middle of the carbachol application, as the patterns tend to be more distorted when carbachol is first added and late into the application as the behavior slows.

Onsets and offsets of activity in the I2 muscle EMG were identified based on the onset and offset of high frequency firing. Activity of I3 was identified based on the activity of the three largest units on the buccal nerve 2 ENG, which have previously been identified by our lab as B3, B6, and B9 (Lu et al, 2013). A subset of the burst onset and offset timings were independently identified by a second researcher to verify inter-rater reliability.

4.5 Numerical methods

The stochastic differential equations were simulated in C++ using an explicit order two weak scheme with additive noise, described in Kloeden and Platen (1992). If the stochastic differential equation is expressed in vector form as

$$dy_t = A(y_t)\,dt + B(y_t)\,dW_t, \tag{31}$$

this scheme is described by the following recurrence relationship:

$$\tilde{y}_{n+1} = y_n + A(y_n)h + B(y_n)\Delta W_n, \tag{32}$$
$$y_{n+1} = y_n + \tfrac{1}{2}(A(\tilde{y}_{n+1}) + A(y_n))h + B(y_n)\Delta W_n. \tag{33}$$

Here h is the length of a time step and ΔW_n is a Weiner increment (a vector of pseudo-random numbers from a Gaussian distribution with mean zero and variance h). Note that in the deterministic case this

reduces to the Heun method (Kloeden and Platen, 1992).

At each time step, any negative values of the a_i state variables were replaced with their absolute value to prevent noise from pushing the system into a non-physiologic range. Random numbers for the Wiener increments were generated using a Mersenne twister with a period of $2^{19937} - 1$ (Matsumoto and Nishimura, 1998). A time step of size 10^{-3} was used. This was verified to be sufficiently small by simulating the model with default parameters and seeing a change in period of less than 30 parts per million (from 4.02704 to 4.02693) when the step size was changed from 10^{-3} to 10^{-4}. Onsets and offsets of bursts were determined by when the activity of the next motor pool rose above the previous one (i.e. $a_{i+1} > a_i$), and were linearly interpolated between time steps to improve accuracy.

5 Results

5.1 Tuning the limit cycle to match the stable heteroclinic channel

Animals in the wild need to adapt their behavior to a changing environment. For example, the marine mollusk *Aplysia* must adapt to the changing forces imposed on it by the stipe of seaweed it is attempting to consume. These forces can vary considerably during the behavior; a stipe of seaweed might initially present very little resistance, but accumulated elastic forces in the seaweed will grow as the animal pulls against the holdfast and tidal forces can present a sudden load with little warning. In addition, these forces can pull the seaweed back out of the animal's mouth during protraction when the grasper is open. This raises the question of which dynamical architecture - the limit cycle or the stable heteroclinic channel - can better adapt to these changing requirements. We therefore explore the efficacy of the limit cycle and the stable heteroclinic channel in the ingestion of seaweed over a range of resisting forces on the seaweed.
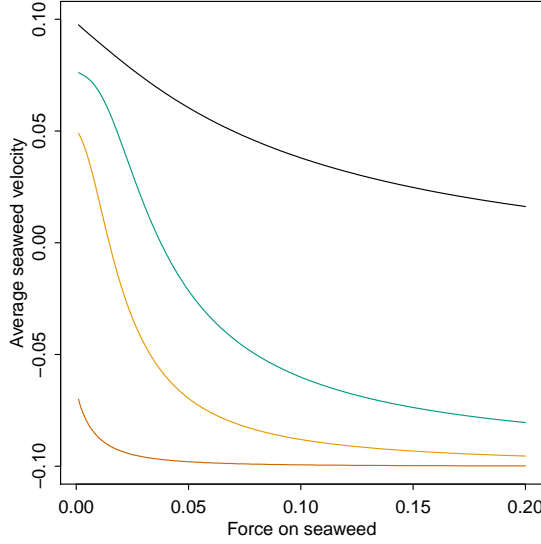
Fig. 4: The limit cycle produced by changing intrinsic neural excitability (μ) alone performs much more poorly than the stable heteroclinic channel, but the limit cycle's performance can be improved by adjustments in timing. Top black line: stable heteroclinic channel. Lower red line: limit cycle produced by only changing μ. Orange line, second from bottom: limit cycle produced by changing μ and τ_n, which controls the overall cycle duration. Green line, third from bottom: limit cycle produced by changing μ and replacing the constant τ_n with the function $\tau_\mathrm{n}(a) = (1 + \alpha \cdot a)\beta$, thus allowing the limit cycle to spend similar times to the stable heteroclinic channel at different phases of the motor pattern.

Although the stable heteroclinic channel model can be changed to a limit cycle by increasing the intrinsic excitability μ, as shown in figure 4 (top line: stable heteroclinic channel ($\mu = 0$), bottom line: limit cycle ($\mu > 0$, all other parameters fixed), the resulting model is unable to effectively ingest seaweed. We thus attempt to tune the parameters for the limit cycle to make it more effective and more comparable to the stable heteroclinic channel. We use the behavior of the stable heteroclinic channel under a light seaweed load ($F_\mathrm{sw} = 0.01$, $b_\mathrm{sw} = 0.10$)

to guide our parameter changes. Under these conditions, the stable heteroclinic channel ingests seaweed at a rate of $0.090/s$, but the limit cycle with changes only to μ *egests* seaweed at a rate of $0.087/s$ (i.e. the seaweed is pulled away more quickly than it can be ingested).

There are a number of reasons why the limit cycle is less effective at ingesting seaweed. The increase in μ dramatically decreases the time spent near the saddles without increasing the time spent moving between saddles; as a result, the period of the neural pattern decreases from $4.03s$ to $0.98s$. To compensate for this change, we increased the time scaling constant τ_n to match the periods. This adjustment increases the efficacy of the limit cycle to ingest at a rate of $0.019/s$; a similar improvement is seen across a range of loads as shown in figure 4, second line from the bottom.

The next obvious cause of the lower efficiency is the length of time each neural pool is active; with the changes to μ and the constant τ_n, each pool is active for nearly equal periods of time (1.35, 1.32, and 1.36 seconds for protraction open, protraction closing, and retraction closed, respectively), whereas in the stable heteroclinic channel, protraction closing ($0.49s$) is much shorter than protraction open and retraction closed ($1.92s$ and $1.61s$). These differences in how long each neural pool is active are likely to be due to differences in sensory responsiveness, which we will explore in section 5.2. In general, a limit cycle could spend different amounts of time in each region of the pattern without requiring dependence on sensory input. To illustrate this point, we adjust the timing of the limit cycle by making τ_n activity dependent, as described in (29), setting β equal to our previous constant τ_n and adjusting the parameter α to make the duration of activity match that seen in the stable heteroclinic channel with the test seaweed load. This increases the efficacy of the limit cycle to $0.067/s$, and again improves the performance of the limit cycle across a range of loads as shown in figure 4, third line from the bottom.

Despite these changes to the intrinsic neural dynamics, the limit cycle is still less effective than the
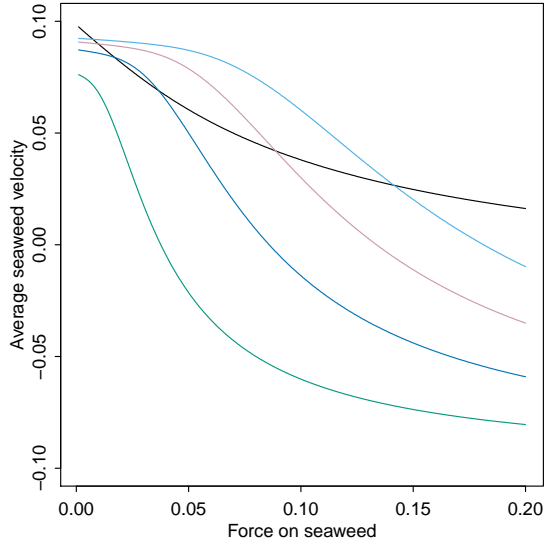
Fig. 5: Increasing the maximum muscle activation allows the limit cycle to perform as well as the stable heteroclinic channel over a range of forces. Black line: stable heteroclinic channel. Bottom green line: limit cycle with timing changes only (matches the green line in figure 4). Dark blue line, second from bottom: limit cycle with timing changes and twice the maximum muscle activation. Violet line, third from bottom: limit cycle with timing changes and three times the maximum muscle activation. Cyan line, fourth from bottom: limit cycle with timing changes and four times the maximum muscle activation.
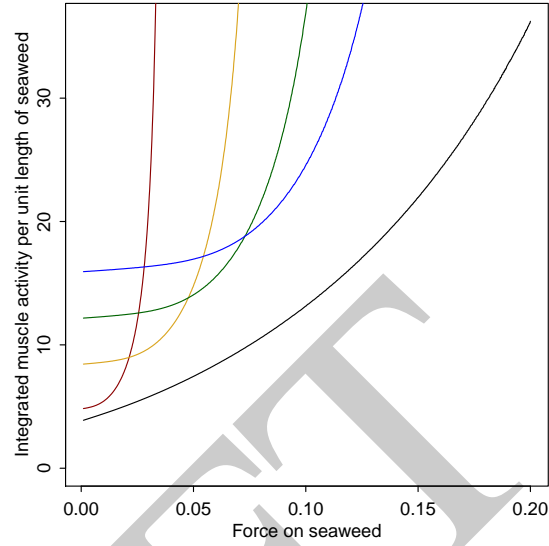

Fig. 6: Increased muscle activation in the limit cycle comes at a metabolic cost. Black line: stable heteroclinic channel. Red line, yellow line, green line, and blue line: limit cycle with timing changes and 1, 2, 3, or 4 times the maximum muscle activation respectively.

stable heteroclinic channel. One reason for this remaining deficit is that the sharp transitions in the stable heteroclinic channel may provide faster activation of the muscles than the more gradual onset and offset of activity in the limit cycle. As shown in figure 5, this slower activation and deactivation can be compensated for by increasing the maximum activation of the muscle (or, equivalently, the cross section of the muscle) u_{max}. Increasing u_{max} by a factor of 2.9 results in a rate of ingestion of 0.090, which is comparable to the efficacy of the stable heteroclinic channel. Note that, as shown in the figure,

even with relatively high values of u_{max}, the stable heteroclinic channel is more effective than the limit cycle when the load on the seaweed is very small or very large.

Although increasing the maximum muscle activation allows the limit cycle to match or even exceed the efficacy of the stable heteroclinic channel over a range of loads, this change has a metabolic cost for the animal. To a first approximation, the energetic cost of contraction is proportional to the force generated by the muscle (Sacco et al, 1994). Thus, under the model's assumption that we are in the linear regime of the force-activation curve, the energetic cost of contraction is also proportional to the activation of the muscle. In figure 6 we show the energetic cost, in the form of integrated muscle activation over time, per length of seaweed ingested. Assuming the
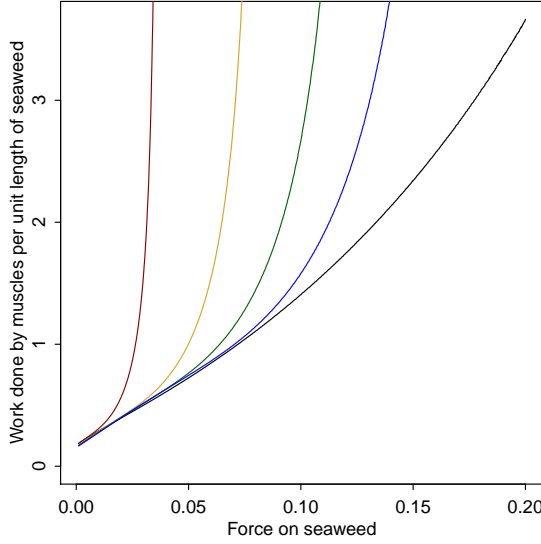
Fig. 7: With higher loads, the limit cycle is less efficient than the stable heteroclinic channel, and does more mechanical work for a given amount of seaweed ingested. Black line: stable heteroclinic channel. Red line, yellow line, green line, and blue line: limit cycle with timing changes and 1, 2, 3, or 4 times the maximum muscle activation respectively.

system has reached steady-state, this is

$$\frac{\int_0^T \sum_i u_i(t)\, dt}{x_{\text{sw}}(0) - x_{\text{sw}}(T)}, \tag{34}$$

where T is the period of the behavior. Note that even at low loads, the limit cycle pays a higher metabolic cost per unit length of seaweed ingested.

The limit cycle's behavior is also mechanically less efficient at higher loads. In figure 7, we show the mechanical work done by the muscles per unit length of seaweed ingested; i.e.

$$\frac{\int_0^T F_{\text{musc}}(s)\, \frac{dx_{\text{r}}}{dt}\Big|_{t=s}\, ds}{x_{\text{sw}}(0) - x_{\text{sw}}(T)}. \tag{35}$$

Note that the limit cycles using more strength are able to remain mechanically efficient over a larger range of forces, but the stable heteroclinic channel is still more mechanically efficient at higher loads

than a limit cycle with muscles that are four times stronger. We will explore the differences in behavior that lead to these effects in the next section.

5.2 Mechanisms of adaptation to load

How do the two architectures adapt to these changes? In figure 8, we can see the changes between low and high seaweed forces. In the limit cycle, the time course of neural activation is very similar under both high and low load conditions. As a result, the forces in the high-load condition dramatically reduce the distance inward that the seaweed is pulled before the odontophore releases the seaweed (thick green line). Note that once the seaweed is released, the retraction force on the odontophore is no longer opposed, and causes a rapid retraction. In the stable heteroclinic channel, by comparison, we can see that the neurons involved in retraction (red) increase their average duration of activity. The resulting long retraction allows the animal to draw in more seaweed by allowing the muscles to exert a greater peak force.

The mechanisms of these changes in timing can be seen in figure 9. In both the stable heteroclinic channel and the limit cycle, the trajectory is moved only a small distance by sensory input. In the case of the limit cycle, the new trajectory passes through a very similar region of phase space as the unperturbed trajectory, and thus the timing of the limit cycle does not change very much. In contrast, in the stable heteroclinic channel, the small perturbation moves the trajectory near the saddle point where the flow changes rapidly even over these short distances. During retraction, the trajectory passes closer to the saddle where the flow is very small; thus it spends longer in this region. Similarly, during protraction, the proprioception of the more protracted radula pushes the trajectory further away from the slow flow near the saddle, thus reducing the amount of time spent in protraction.

It is natural to ask whether the intact behaving animal employs similar strategies. Because it is difficult in the intact animal to assess the dynamic forces generated by seaweed bunching up in the buccal cav-
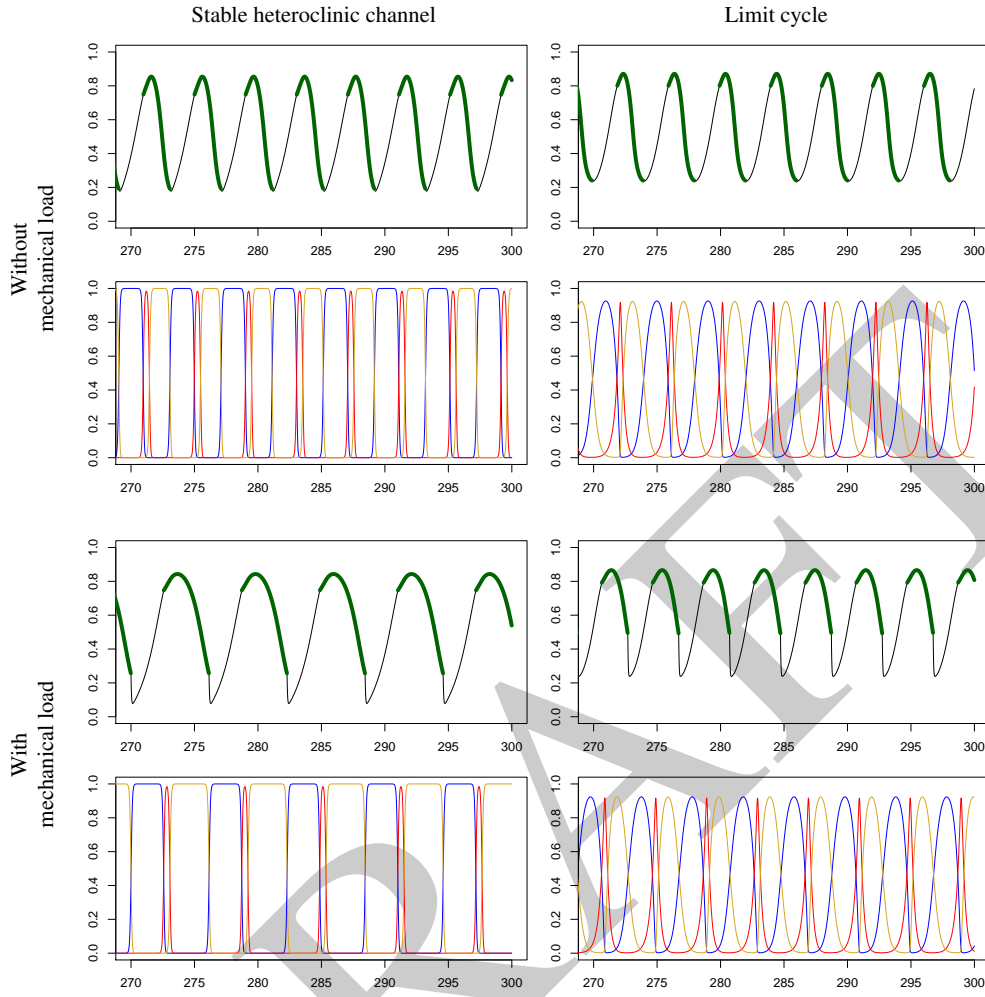
Fig. 8: Forces on seaweed can selectively prolong the retraction phase of the stable heteroclinic channel, but have little effect on the limit cycle. Black and green lines show the position of the radula-odontophore, with the thick green sections showing the positions when the odontopore is closed on the seaweed and the black sections showing the positions when the odontophore is open. The blue, gold and red lines show the activity of the protraction open, protraction closing, and retraction closed motor pools, respectively. For the mechanical load, F_{sw} was increased to 0.1 and b_{sw} was increased to 1.0. The positions of the odontophore are similar for both the stable heteroclinic channel and the limit cycle when there is little load. Note that the duration of retraction closed (gold) increases substantially in the stable heteroclinic channel under load, resulting in a greater retraction while holding the seaweed, but not in the limit cycle under load.

Stable Heteroclinic Channel   Limit cycle
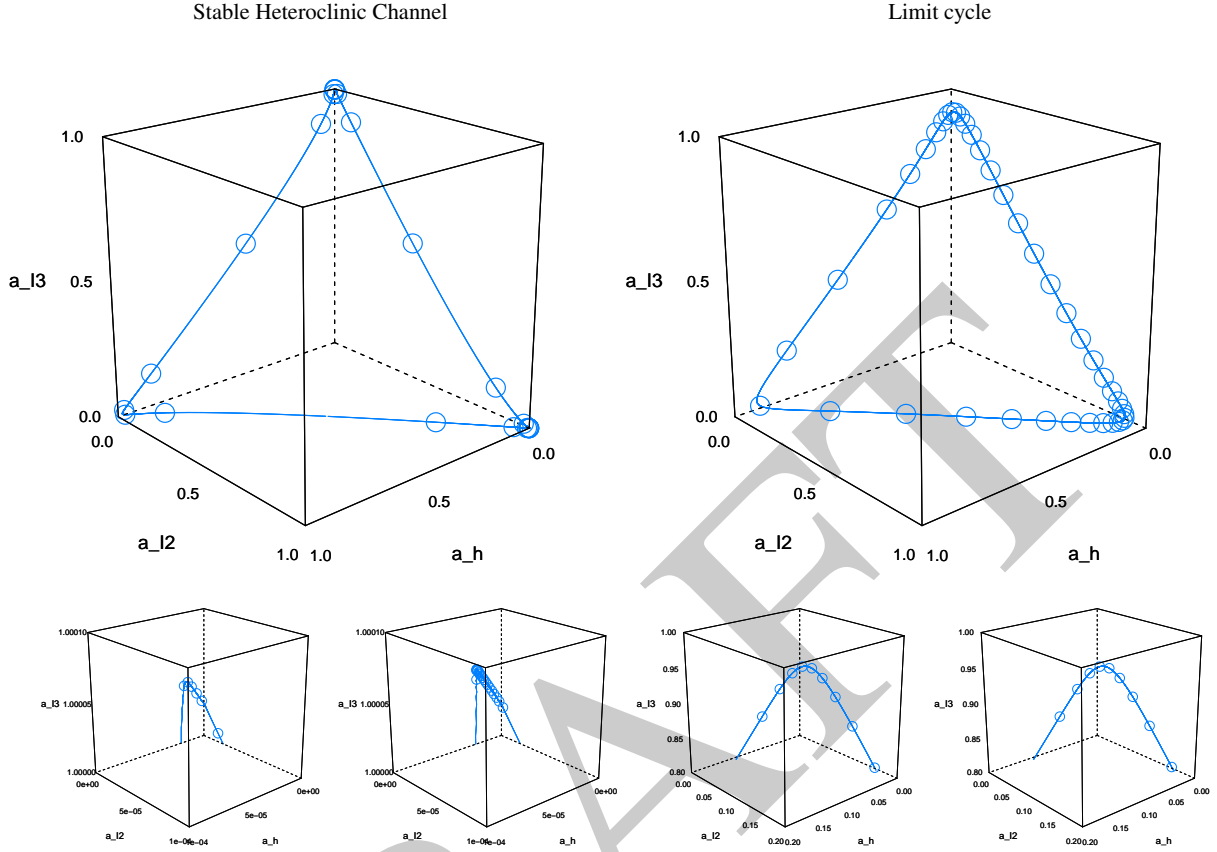

Fig. 9: A small change in the trajectory caused by sensory input can have a large effect on the timing of the stable heteroclinic channel by pulling the trajectory closer to the saddle; the same magnitude of change has very little effect on the limit cycle. The upper row shows the trajectory of the neural variables in phase space with no load present for both the stable heteroclinic channel and the limit cycle. The circles represent points equally spaced in time (by 100 ms) to provide a sense of the velocity of the trajectory. When the force exerted by the seaweed is increased ($F_{sw} = 0.1$, $b_{sw} = 1.0$), the position of the trajectory changes only a small amount. To show this, the lower row contains a magnification of the top corner of the trajectory (where the retraction-closed motor pool is most active) for the stable heteroclinic channel with the light (0.01) and heavy (0.1) mechanical load, and the limit cycle with the same two loads. The stable heteroclinic channel plots are magnified by 10000 times, whereas the limit cycle plots are magnified by 10 times.

ity as seaweed is ingested, we consider a simplified situation where a stiff elastic force is encountered during a swallow that prevents the seaweed from moving inward, such as the holdfast of the seaweed. In the model, this resistance can be simulated by attaching a stiff spring to the seaweed. We can create the analagous situation in the animal by feeding the animal a thin strip of seaweed and then holding the seaweed during a swallow to present a resisting force.

The resulting change to the pattern, shown in figure 10, is very similar to what was seen with a constant force applied to the seaweed: again retraction duration lengthens and protraction duration shortens.

How do these strategies compare to those used by the animal itself? As shown in figure 11, the duration of retraction increases, although the duration of protraction does not appear to increase or decrease. It is possible that the additional strategies used by the animal, such as moving the head, allowed the animal to fully retract and thus negated the need for shorter protractions.

It is not surprising that an animal would behave in an adaptive manner to the behaviorally relevant task of consuming seaweed. If the dynamics of the central nervous system are stable heteroclinic channel-like, would this create any changes that would not be expected from a purely adaptive standpoint? There are two we will discuss here: the response to removal of proprioception and the shape of the distribution of durations of components of the pattern.

The effects of removing sensory input are different for the limit cycle and the stable heteroclinic channel as shown in figure 12. In a limit cycle, the dynamics of the pattern generator produce a well formed pattern even in the absence of sensory input. In an stable heteroclinic channel, in contrast, normal patterns are only generated when sensory input pushes the trajectories away from the saddles. When sensory input is reduced, the trajectory passes much closer to the saddles and all parts of the pattern that are responsive to sensory input will be lengthened. In a deterministic system with a precisely tuned stable heteroclinic channel (so that the cycle is a true

heteroclinic cycle that includes the saddle points), the duration of patterns will grow without bound. In a more realistic scenario, however, small amounts of noise and small imperfections in tuning of the cycle will lead to longer, but still finite, cycle times. In figure 12, we thus set the noise η to 10^{-30} to show that even a very small amount of noise is sufficient to prevent the stable heteroclinic channel from becoming "stuck" in one of the phases.

When sensory input is removed from the animal, does the duration of protraction and retraction increase as is seen in the stable heteroclinic channel, or remain about the same as is seen in the limit cycle? To investigate this, we examine two preparations of the animal with reduced sensory input and compare them to the intact animal. In the first preparation, the suspended buccal mass(McManus et al, 2012), the feeding apparatus and the ganglia controlling feeding are dissected out of the animal and suspended in a saline solution. This preparation thus removes sensory input the animal would have gotten from the lips, anterior tentacles, and other parts of the body, but not the proprioceptive feedback from the feeding apparatus itself. In the second preparation, the isolated ganglia, the feeding apparatus is also dissected away, leaving just the ganglia controlling feeding. As shown in figure 13, protraction (containing both the protraction open and protraction closing phases) and retraction (closed) both increase in duration from the intact animal to the suspended buccal mass, and increase further in duration from the suspended buccal mass to the fictive patterns of the isolated ganglia. Note that this increase in both protraction and retraction differs from the selective increase in retraction when the seaweed was held in figure 11, but matches the increase in both phases seen in the stable heteroclinic channel.

When subject to small amounts of noise, the stable heteroclinic channel and the limit cycle show different forms of variability in timing. In the limit cycle, perturbations from the noise have very similar effects regardless of where they occur in the cycle, so, by the central limit theorem, their cumulative effect is approximately Gaussian in the limit of small
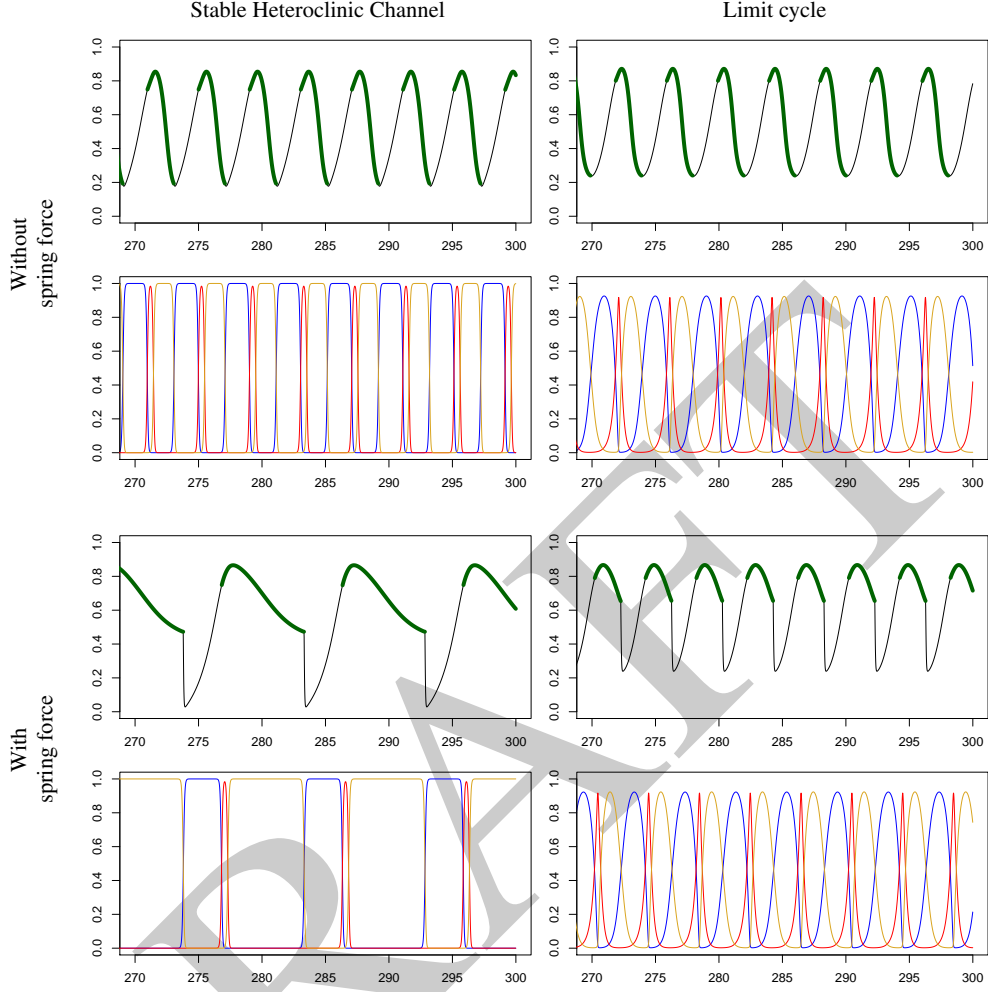
Fig. 10: A spring resisting retraction can selectively prolong the retraction phase of the stable heteroclinic channel, but has little effect on the limit cycle. For the "with spring force" plots, F_{sw} is defined by (26) with $k_{spring} = 2.0$ and $x_{spring} = 0.9$; parameters are otherwise as described in table 1. Line colors are the same as those in figure 8.

noise[2]. In contrast, as described in Shaw et al (2012), perturbations that occur while approaching the saddle can have much larger effects than perturbations

that occur while leaving the saddle, so the central limit theorem does not apply. As predicted by Stone and Holmes (1990), this results in a distribution that is skewed to the left. The result of simulations with noise, shown in figure 14, is that the distribution for the stable heteroclinic channel is significantly skewed compared to the more symmetric distribution for the limit cycle. If we look at the duration of

---

[2] In the limit cycle, the time spent passing through one part of the cycle can be approximated as the first passage time of a Brownian particle with drift, so the small noise assumption is important; the distribution will become skewed as the noise becomes large relative to the drift.
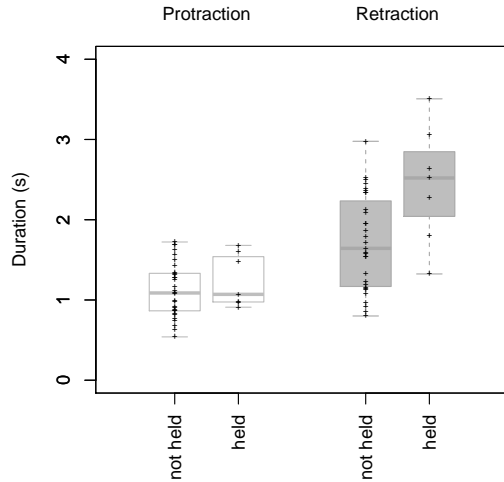
Fig. 11: When a force is applied to the seaweed *in vivo* (by holding the seaweed), the activity of the neurons involved in retraction (corresponding to retraction closed) is prolonged (right), while the activity of the protractor muscle (corresponding to the start of protraction open to the end of protraction closing) is not (left). Medians differ (Mann–Whitney test, $p = 0.013$), 30 unheld swallows and 7 held swallows were used from the same two animals. Results are similar if unheld swallows from all 6 animals are used (not shown, $p = 0.003$).

retraction in swallows in the intact animal, shown in figure 15, we see that the distribution is significantly skewed, more closely resembling that seen in the stable heteroclinic channel domain of the model.

6 Discussion

In this paper, we have examined a neuromechanical model of feeding in *Aplysia* in two parameter regimes. In the first parameter regime, the pattern generator acts like an idealized central pattern generator, generating a physiologically efficient pattern in the absence of sensory input. In the second parameter regime, which has dynamics more similar to those

of a chain reflex, passage near saddle points leads to greater sensitivity to sensory inputs, and the system generates very distorted patterns in the absence of sensory input.

We have shown that the model based on an idealized central pattern generator does not adapt as well to changing loads as the model based on the stable heteroclinic channel does. We showed that part of this change is due to a prolongation of retraction allowing greater activation of the slow retractor muscles. We then showed that the animal itself appears to use the same strategy of prolonging retraction when faced with loads *in vivo*.

We showed that the stable heteroclinic channel provided a better match to the biological data than the idealized central pattern generator, even for aspects of the behavior that do not convey an obvious evolutionary advantage. The first example, removal of sensory feedback, showed increased slowing in the animal and the stable heteroclinic channel, rather than the near-constant timing predicted by the idealized central pattern generator. The second example, distribution of burst durations, showed a very skewed distribution both in vivo and in vitro, compared to the much less skewed distribution predicted by the model with the idealized central pattern generator.

6.1 Limitation of the model and results

We have intentionally created a very nominal model of feeding behavior which does not capture many of the details known about feeding in *Aplysia*.

As previous work from our lab and others has shown, there are many degrees of biomechanical freedom beyond protraction and retraction that influence the efficacy of feeding (Sutton et al, 2004a,b; Novakovic et al, 2006), the muscles involved have many properties which we do not include in our model (Yu et al, 1999; Zajac, 1989), and the mechanics of seaweed are much more complex than we have represented in the model (Denny and Gaylord, 2002; Harder et al, 2006). Similarly, the dynamics of proprioception are much more complex than the linear model we have used (Evans and Cropper, 1998), and
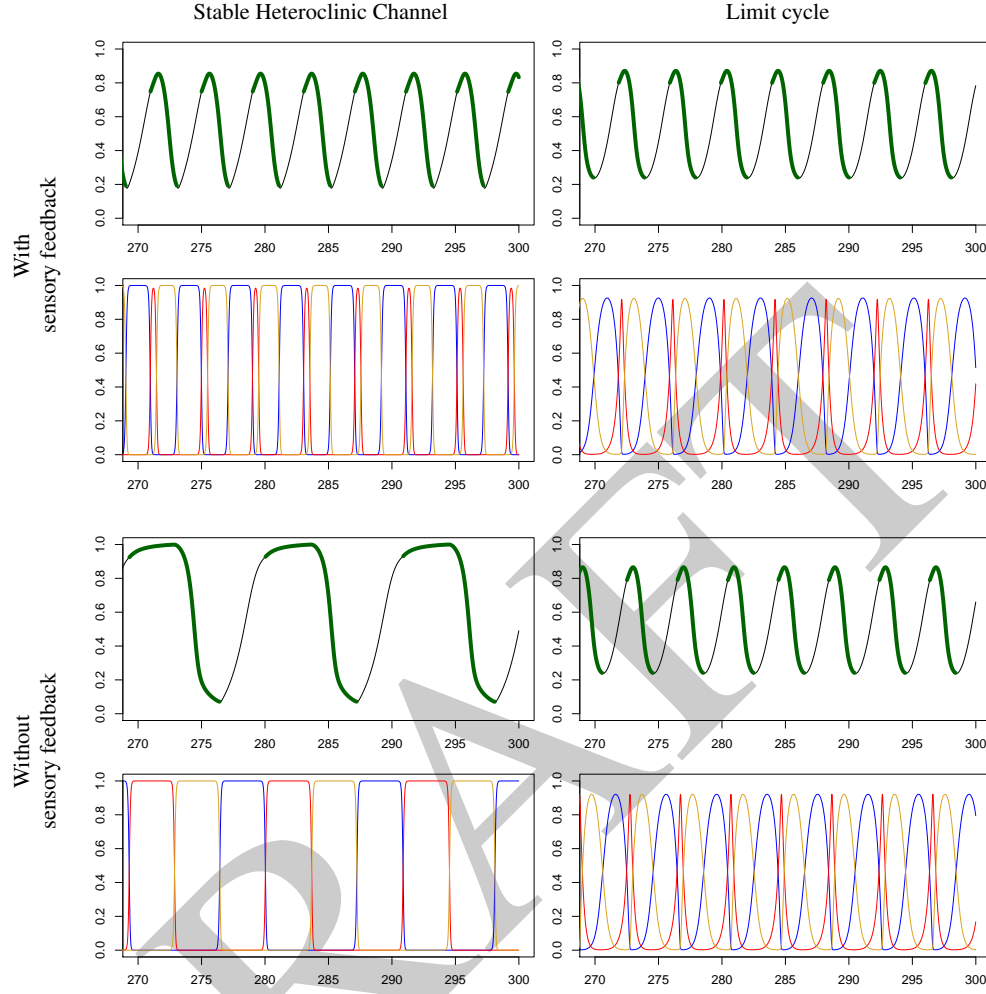
Fig. 12: Removing sensory feedback slows both protraction and retraction in the stable heteroclinic channel, but has little effect on the limit cycle. For plots without sensory feedback, $\varepsilon = 0$ and $\eta = 10^{-30}$; parameters are otherwise as described in table 1.

there are more than three pools of neurons involved in feeding behavior (Hurwitz et al, 1997), with dynamics that are much more complex than the firing rate model we have used (Susswein et al, 2002). In addition, neuromodulation and learning may alter the dynamics of the network slowly over time (Nargeot and Simmers, 2012; Susswein and Chiel, 2012). Thus we expect at best a qualitative match to the *in vivo* behavior, and can not compare the results

against other models as rigorously as could be done with a model capable of quantitative predictions.

A nominal model also has advantages, however. As complexity is added to a model, it can become more difficult to interpret the mechanics and, as a result, less clear what details of the dynamics are responsible for an observed aspect of the behavior. In addition, as the parameter space grows it becomes less obvious how dependent the results are on the par-
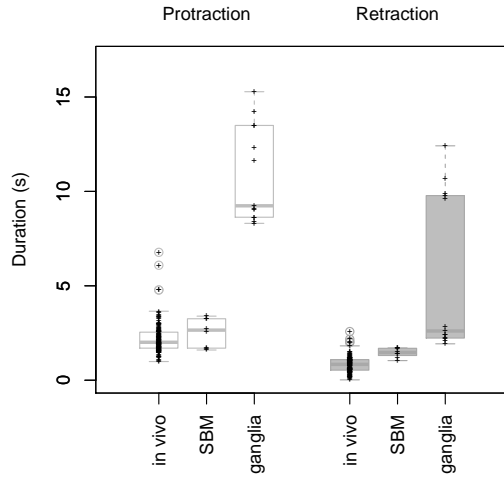
Fig. 13: Protraction and retraction intervals are longer in the suspended buccal mass than in the intact animal, and longer in the isolated ganglia than in either the suspended buccal mass or the intact animal. Bites were used (rather than swallows) because there is no clear analog of a swallow in the isolated ganglia. Medians differ significantly by preparation type for both protraction (Kruskal–Wallis, $p < 0.001$) and retraction (Kruskal–Wallis, $p < 0.001$). Results are similar when swallows from the *in vivo* and suspended buccal mass preparations are used instead of bites (not shown, $p < 0.001$ for both protraction and retraction). Recordings *in vivo*: 146 bites from 6 animals. Suspended buccal mass: 8 bites from 2 animals. Isolated ganglia: 13 motor patterns from 2 animals.
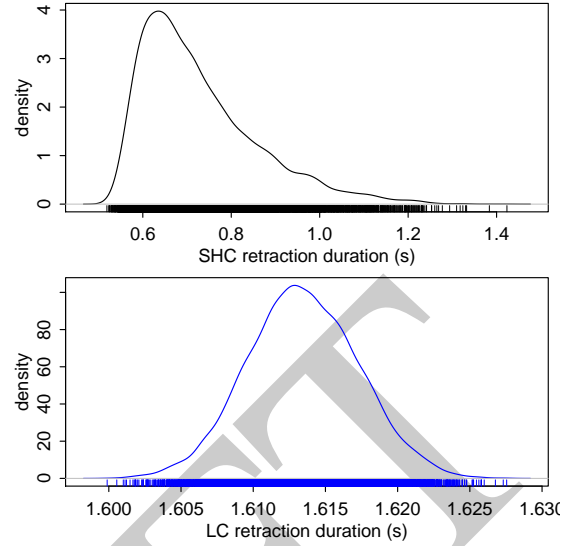

Fig. 14: In the presence of small amounts of noise, retractions are significantly more skewed for the stable heteroclinic channel than for the limit cycle (skewness = 0.91 vs 0.03, for the stable heteroclinic channel and limit cycle respectively. D'Agostino test for skewness(D'Agostino et al, 1990): $\sqrt{b_1} = 32$ vs 1.1, $p < 0.001$ vs $p = 0.27$). Shown is the kernel density estimator for the last a_{I3} duration in each of 10000 simulations with noise $\eta = 10^{-4}$.

ticular choice of parameters (Foster et al, 1993). Thus the nominal model we have used makes it clearer that the effects we see are caused by the effects of sensory perturbations on the passage near a saddle point, and the role of the parameters in creating these dynamics can be easily understood in an intuitive manner.

In addition, the dynamics we have included in the model (e.g. mutually inhibitory motor pools, slow muscle antagonistic muscles, and a slow muscle

transfer function) are all dynamics that are common to many other systems. Thus our results about the qualitative behavior of the model clearly may be applicable to these other systems, which would not be as clear with a more specialized model.

It is possible that some of these omitted details are critical for producing the observed behavior and that the simpler dynamics we are using may not represent the behavior of the actual system. For example, in our model the passage near a saddle, where the state variables are changing slowly, corresponds to a burst in the actual behavior where some state variables (e.g. membrane potential and gating variables) are changing quickly. Many such systems, however, can be decomposed into fast and slow subsystems, (Butera et al, 1996; Krupa et al, 2008; Sherwood and
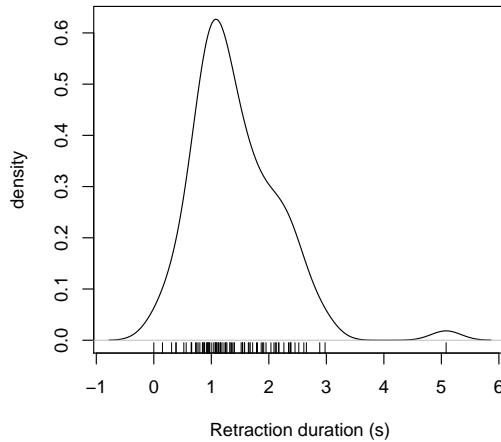
Fig. 15: Retraction durations are significantly skewed during swallowing patterns in intact *Aplysia californica* (skewness = 1.4, D'Agostino test for skewness(D'Agostino et al, 1990): $\sqrt{b_1} = 4.56$, $p < 0.001$). Shown is the kernal density estimator of the total duration of B6/B9 and B3 activity from 84 swallowing patterns in 6 animals.

Guckenheimer, 2010), and these slow passages near saddles may occur in the dynamics of the slow state variables, as has been seen by Nowotny and Rabinovich (2007). Ideally, one would want to create a more detailed model of feeding in *Aplysia*, and then use a principled reduction to find the slower dynamics. The work done in this paper may be useful for guiding such a reduction.

6.2 Larger implications for pattern generators

6.2.1 Biological aspects

Many previous authors have noted the difference between patterns seen *in vitro* and those seen *in vivo*, but the field has not yet reached a consensus about the source of these differences. In this paper, we propose that passage of trajectories near a fixed point

provides a model that can explain some of the distortions in timing seen *in vitro*. Furthermore, this dynamical structure may help a pattern generator better use sensory input to adapt to a changing environment, and thus this structure may be selected for by evolutionary pressures. Although stable heteroclinic cycles are not structurally stable and thus are unlikely to be seen in a biological context, stable heteroclinic channels *are* structurally stable and thus robust to parameter variations and noise (Afraimovich et al, 2004), and thus are plausible dynamics for a biological system. This emergence of passage near fixed points controlling timing has been seen in other models, for example Spardy et al (2011).

Many other pattern generators that have been previously identified may lie between the two extremes on this continuum between ideal central pattern generators and chain reflexes. Slower patterns in the absence of innervation have been seen in lamprey swimming (Wallén and Williams, 1984), crayfish walking (Chrachri and Clarac, 1990), and locust flight (Pearson et al, 1983).

These models of pattern generation may also be relevant in clinical contexts. In mammals, fictive respiration can be observed in the isolated central nervous system, and is hypothesized to arise from the interaction of two pattern generators in the medulla - an inspiratory pattern generator in the pre-Botzinger complex, and an expiratory pattern generator in the retrotrapezoidal-parafacial area (Tomori et al, 2010). It has been known for some time, however, that vagotomy (cutting the vagus nerve, which contains sensory afferents involved in respiration) causes a dramatic slowing, but not cessation of respiration. Qualitatively this behavior is much closer to what we have shown in the stable heteroclinic channel model, and not that of the idealized limit cycle. This would suggest that small perturbations may be enough to cause the changes seen in central sleep apnea and possibly sudden infant death syndrome, but also suggests that the system may remain quite sensitive to certain perturbations even in the pathological state. In the case of central sleep apnea, good models of the dynamics and sensitivity might allow for new treatment modal-

ities such as transcranial direct current stimulation during episodes of apnea or hypopnea.

6.2.2 Mathematical implications

Many of the behaviors we have observed in the stable heteroclinic channel may depend primarily on localized regions of the dynamics where the intrinsic dynamics, $f(a, \mu)$, are comparable in magnitude to $\varepsilon g(a, x)$. When this is not the case, the sensory input will have little effect on the speed of the trajectory, and thus can only cause large changes in timing by dramatically changing the length of the trajectory.

Although we have used a stable heteroclinic channel in our model to create localized regions of slowing, several related dynamics architectures may produce similar effects. For example, in a saddle-node bifurcation on an invariant cycle, the flow around a limit cycle slows near a point as one approaches the bifurcation. This slowing may create qualitatively similar behavior[3]. Other examples may include relaxation oscillators where some parts of the trajectory are much slower than others, e.g. van der Pol (1926), which can create similar regions of sensitivity (Bässler, 1986).

These localized regions of slowing may not always be apparent in the model as written. For example, many dynamical models, such as bursting cells, may not have localized regions of slowing in the form that they are written, but can be decomposed using fast-slow analysis into state variables that change on different time scales. In these systems, saddle points may exist in the slower state variables that were not apparent in the complete system.

Feldman (1966) introduced the hypothesis that motor trajectories could be understood as the result of a control process that sets up one or a sequence of biomechanical equilibrium points. Typically, the control is set by an unspecified central mechanism that may take into account high-level sensory (visual, auditory) or goal-related information.

Our framework is consistent with the Equilibrium Point Hypothesis (EPH) when the system (1 - 2) has ε set to zero, the autonomous central dynamics has a fixed point $f(a_{\text{target}}, \mu) = 0$ for which the target configuration, x_{target}, is a fixed point of the biomechanics, i.e. $h(a_{\text{target}}, x_{\text{target}}) = 0$, with a suitable adjustment in the case of a nonzero load. The incorporation of sensory feedback from the motor apparatus is not explicitly included in the EPH, although it is implicit in the setting of the neural equilibrium point.

Because of the key role of sensory sensitivity demonstrated in this paper, it is natural to ask what can be said more generally for systems of the form (1-2). For weak proprioceptive input and/or weak mechanical forcing, the phase response curves of the isolated neural dynamics, (1) with $\varepsilon = 0$, and the neural dynamics coupled to the periphery, (1-2), could be expected to play a role. It is not clear how the two phase response curves are related, particularly in the case of the stable heteroclinic channel for which the uncoupled system does not have a finite period limit cycle and therefore does not have a well defined phase. However, as we have shown elsewhere (Shaw et al, 2012) one can analyze the infinitesimal phase response curve for the limit cycle obtained in the limit of small μ, and the infinitesimal phase response curve diverges in a systematic fashion for phases intermediate between successive saddle points. This large sensitivity could play a role in making stable heteroclinic channels a more sensitive dynamical architecture for incorporating guidance of motor systems via modest sensory input signals – as in the boundary between the typical limit cycle and the chain reflex.

References

Afraimovich V, Young T, Muezzinoglu MK, Rabinovich MI (2011) Nonlinear dynamics of emotion-cognition interaction: When emotion does not destroy cognition? Bulletin of Mathematical Biology 73(2):266–284, DOI 10.1007/s11538-010-9572-

---

[3] The similarity actually goes deeper than this; if one adds a new state variable representing the bifurcation parameter μ and sets $d\mu/dt = 0$, the limit cycle in the augmented system now passes near a degenerate saddle at $\mu = 0$.

x, URL http://link.springer.com/article/10.1007/
s11538-010-9572-x

Afraimovich VS, Zhigulin VP, Rabinovich MI (2004)
On the origin of reproducible sequential activity in neural circuits. Chaos: An Interdisciplinary Journal of Nonlinear Science 14(4):1123, DOI 10.1063/1.1819625, URL http://link.aip.org/link/CHAOEH/v14/i4/p1123/s1&Agg=doi

Bakhtin Y (2011) Noisy heteroclinic networks. Probability Theory and Related Fields 150(1-2):1–42, DOI 10.1007/s00440-010-0264-0, URL http://link.springer.com/article/10.1007/s00440-010-0264-0

Baxter DA, Byrne JH (2006) Feeding behavior of *Aplysia*: A model system for comparing cellular mechanisms of classical and operant conditioning. Learn Mem 13(6):669–680, DOI 10.1101/lm.339206, URL http://www.learnmem.org/cgi/content/abstract/13/6/669

Butera RJ, Clark JW, Byrne JH, Rinzel J (1996) Dissection and reduction of a modeled bursting neuron. Journal of Computational Neuroscience 3(3):199–223, DOI 10.1007/BF00161132, URL http://www.springerlink.com/content/n2733052qjgj5761/

Bässler U (1986) On the definition of central pattern generator and its sensory control. Biological Cybernetics 54(1):65–69, DOI 10.1007/BF00337116, URL http://link.springer.com/article/10.1007/BF00337116

Cataldo E, Byrne J, Baxter D (2006) Computational model of a central pattern generator. In: Computational Methods in Systems Biology, Lecture Notes in Computer Science, vol 4210, Springer Berlin / Heidelberg, pp 242–256, URL http://dx.doi.org/10.1007/11885191_17

Chrachri A, Clarac F (1990) Fictive locomotion in the fourth thoracic ganglion of the crayfish, *Procambarus clarkii*. The Journal of Neuroscience 10(3):707–719, URL http://www.jneurosci.org/content/10/3/707

Church PJ, Lloyd PE (1994) Activity of multiple identified motor neurons recorded intracel-

lularly during evoked feedinglike motor programs in *Aplysia*. J Neurophysiol 72(4):1794–1809, URL http://jn.physiology.org/cgi/content/abstract/72/4/1794

Cullins MJ, Chiel HJ (2010) Electrode fabrication and implantation in *Aplysia californica* for multi-channel neural and muscular recordings in intact, freely behaving animals. Journal of Visualized Experiments (40), DOI 10.3791/1791, URL http://www.jove.com/video/1791/electrode-fabrication-implantation-aplysia-californica-for-multi

D'Agostino RB, Belanger A, D'Agostino RB (1990) A suggestion for using powerful and informative tests of normality. The American Statistician 44(4):316–321, DOI 10.2307/2684359, URL http://www.jstor.org/stable/2684359

Denny M, Gaylord B (2002) The mechanics of wave-swept algae. Journal of Experimental Biology 205(10):1355–1362, URL http://jeb.biologists.org/content/205/10/1355

Evans CG, Cropper EC (1998) Proprioceptive input to feeding motor programs in *Aplysia*. J Neurosci 18(19):8016–8031, URL http://www.jneurosci.org/cgi/content/abstract/18/19/8016

Feldman AG (1966) Functional tuning of the nervous system with control of movement or maintenance of a steady posture. II. controllable parameters of the muscle. Biophysics 11(3):565–578

Forssberg H (1979) Stumbling corrective reaction: a phase-dependent compensatory reaction during locomotion. Journal of Neurophysiology 42(4):936–953, URL http://jn.physiology.org/content/42/4/936

Forssberg H, Grillner S, Rossignol S (1975) Phase dependent reflex reversal during walking in chronic spinal cats. Brain Research 85(1):103–107, URL http://journals.ohiolink.edu/ejc/article.cgi?issn=00068993&issue=v85i0001&article=103_pdrrdwicsc

Foster WR, Ungar LH, Schwaber JS (1993) Significance of conductances in Hodgkin-Huxley models. Journal of Neurophysiology 70(6):2502–2518,

URL http://jn.physiology.org/content/70/6/2502

Fox LE, Lloyd PE (1997) Serotonin and the small cardioactive peptides differentially modulate two motor neurons that innervate the same muscle fibers in *Aplysia*. The Journal of Neuroscience 17(16):6064–6074, URL http://www.jneurosci.org/content/17/16/6064

Goldwyn JH, Shea-Brown E (2011) The what and where of adding channel noise to the Hodgkin-Huxley equations. PLoS Comput Biol 7(11):e1002,247, DOI 10.1371/journal.pcbi.1002247, URL http://dx.doi.org/10.1371/journal.pcbi.1002247

Gordon AM, Huxley AF, Julian FJ (1966) The variation in isometric tension with sarcomere length in vertebrate muscle fibres. The Journal of Physiology 184(1):170–192, URL http://jp.physoc.org/content/184/1/170

Guckenheimer J, Holmes P (1988) Structurally stable heteroclinic cycles. Mathematical Proceedings of the Cambridge Philosophical Society 103(01):189–192, DOI 10.1017/S0305004100064732

Harder DL, Hurd CL, Speck T (2006) Comparison of mechanical properties of four large, wave-exposed seaweeds. American Journal of Botany 93(10):1426–1432, DOI 10.3732/ajb.93.10.1426, URL http://www.amjbot.org/content/93/10/1426

Harri M, Florey E (1977) The effects of temperature on a neuromuscular system of the crayfish, *Astacus leptodactylus*. Journal of comparative physiology 117(1):47–61, DOI 10.1007/BF00605523, URL http://link.springer.com/article/10.1007/BF00605523

Hurwitz I, Neustadter D, Morton DW, Chiel HJ, Susswein AJ (1996) Activity patterns of the B31/B32 pattern initiators innervating the I2 muscle of the buccal mass during normal feeding movements in *Aplysia californica*. Journal of Neurophysiology 75(4):1309–26

Hurwitz I, Kupfermann I, Susswein AJ (1997) Different roles of neurons B63 and B34 that are active during the protraction phase of buccal motor programs in *Aplysia californica*. Journal of Neurophysiology 78(3):1305 –1319, URL http://jn.physiology.org/content/78/3/1305.abstract

Ijspeert AJ (2008) Central pattern generators for locomotion control in animals and robots: A review. Neural Networks 21(4):642–653, DOI 10.1016/j.neunet.2008.03.014, URL http://www.sciencedirect.com/science/article/B6T08-4SH6B9F-2/2/2e0a2fdad02d315becc218a6602f054d

Kloeden PE, Platen E (1992) Numerical solution of stochastic differential equations. Springer-Verlag, Berlin

Krupa M, Popović N, Kopell N, Rotstein HG (2008) Mixed-mode oscillations in a three time-scale model for the dopaminergic neuron. Chaos: An Interdisciplinary Journal of Nonlinear Science 18(1):015,106–015,106–19, DOI doi:10.1063/1.2779859, URL http://chaos.aip.org/resource/1/chaoeh/v18/i1/p015106_s1

Levi R, Varona P, Arshavsky YI, Rabinovich MI, Selverston AI (2004) Dual sensory-motor function for a molluskan statocyst network. J Neurophysiol 91(1):336–345, DOI 10.1152/jn.00753.2003, URL http://jn.physiology.org/cgi/content/abstract/91/1/336

Lewinger WA, Rutter BL, Blümel M, Büschges A, Quinn RD (2006) Sensory coupled action switching modules (SCASM) generate robust, adaptive stepping in legged robots. In: Proceedings of the 9th International Conference on Climbing and Walking Robots (CLAWAR'06), Brussels, Belgium, September 12-14, p 661–71

Loeb J (1899) Einleitung in die vergleichende Gehirnphysiologie und vergleichende psychologie, mit besonderer berücksichtigung der wirbellosen thiere. Leipzig, J. A. Barth, URL http://archive.org/details/einleitungindiev00loeb

Lu H, McManus JM, Chiel HJ (2013) Extracellularly identifying motor neurons for a muscle motor pool in *Aplysia californica*. Journal of Visualized Experiments (73), DOI 10.3791/50189, URL http://www.jove.com/video/50189/extracellularly-identifying-motor-neurons-for-muscle-motor-pool

Marder E, Bucher D (2001) Central pattern generators and the control of rhythmic movements. Current Biology 11(23):R986–R996, DOI 10.1016/S0960-9822(01)00581-4, URL http://www.sciencedirect.com/science/article/pii/S0960982201005814

Matsumoto M, Nishimura T (1998) Mersenne twister: a 623-dimensionally equidistributed uniform pseudo-random number generator. ACM Trans Model Comput Simul 8(1):3–30, DOI 10.1145/272991.272995, URL http://doi.acm.org/10.1145/272991.272995

McManus JM, Lu H, Chiel HJ (2012) An in vitro preparation for eliciting and recording feeding motor programs with physiological movements in *Aplysia californica*. Journal of Visualized Experiments (70), DOI 10.3791/4320, URL http://www.jove.com/video/4320/an-vitro-preparation-for-eliciting-recording-feeding-motor-programs

Morton DW, Chiel HJ (1993) The timing of activity in motor neurons that produce radula movements distinguishes ingestion from rejection in *Aplysia*. Journal of Comparative Physiology A: Neuroethology, Sensory, Neural, and Behavioral Physiology 173(5):519–536, DOI 10.1007/BF00197761, URL http://dx.doi.org/10.1007/BF00197761

Nargeot R, Simmers J (2012) Functional organization and adaptability of a decision-making network in *Aplysia*. Frontiers in Neuroscience 6, DOI 10.3389/fnins.2012.00113, URL http://www.ncbi.nlm.nih.gov/pmc/articles/PMC3405415/

Neustadter DM, Drushel RF, Chiel HJ (2002) Kinematics of the buccal mass during swallowing based on magnetic resonance imaging in intact, behaving *Aplysia californica*. Journal of Experimental Biology 205(7):939–958, URL http://jeb.biologists.org/cgi/content/abstract/205/7/939

Neustadter DM, Herman RL, Drushel RF, Chestek DW, Chiel HJ (2007) The kinematics of multifunctionality: comparisons of biting and swallowing in *Aplysia californica*. Journal of Experimental Biology 210(2):238–260, DOI 10.1242/jeb.02654, URL http://jeb.biologists.org/cgi/content/abstract/210/2/238

Novak B, Csikasz-Nagy A, Gyorffy B, Nasmyth K, Tyson JJ (1998) Model scenarios for evolution of the eukaryotic cell cycle. Philosophical Transactions of the Royal Society of London Series B: Biological Sciences 353(1378):2063–2076, DOI 10.1098/rstb.1998.0352, URL http://rstb.royalsocietypublishing.org/content/353/1378/2063

Novakovic VA, Sutton GP, Neustadter DM, Beer RD, Chiel HJ (2006) Mechanical reconfiguration mediates swallowing and rejection in *Aplysia californica*. Journal of Comparative Physiology A: Neuroethology, Sensory, Neural, and Behavioral Physiology 192(8):857–870, DOI 10.1007/s00359-006-0124-7, URL http://dx.doi.org/10.1007/s00359-006-0124-7

Nowotny T, Rabinovich MI (2007) Dynamical origin of independent spiking and bursting activity in neural microcircuits. Physical Review Letters 98(12):128,106–4, DOI 10.1103/PhysRevLett.98.128106, URL http://link.aps.org/abstract/PRL/v98/e128106

Pearson KG, Reye DN, Robertson RM (1983) Phase-dependent influences of wing stretch receptors on flight rhythm in the locust. J Neurophysiol 49(5):1168–1181, URL http://post.queensu.ca/ locust/Publications/pearson%20reye%20robertson%201983%20jnp.pdf

van der Pol B (1926) On "relaxation-oscillations". Philosophical Magazine Series 7 2(11):978–992, DOI 10.1080/14786442608564127, URL http://www.tandfonline.com/doi/abs/10.1080/14786442608564127

Rabinovich MI, Huerta R, Varona P, Afraimovich VS (2008) Transient cognitive dynamics, metastability, and decision making. PLoS Comput Biol 4(5):e1000,072, DOI 10.1371/journal.pcbi.1000072, URL http://dx.plos.org/10.1371/journal.pcbi.1000072

Reyn JW (1980) Generation of limit cycles from separatrix polygons in the phase plane. In: Martini R (ed) Geometrical Approaches to Differential Equations, no. 810 in Lecture Notes in

Mathematics, Springer Berlin Heidelberg, pp 264–289, URL http://link.springer.com/chapter/10.1007/BFb0089983

Sacco P, McIntyre DB, Jones DA (1994) Effects of length and stimulation frequency on fatigue of the human tibialis anterior muscle. Journal of Applied Physiology 77(3):1148–1154, URL http://jap.physiology.org/content/77/3/1148

Schiff SJ (2012) Neural control engineering: the emerging intersection between control theory and neuroscience. MIT Press, Cambridge, MA, URL http://search.ebscohost.com/login.aspx?direct=true&scope=site&db=nlebk&db=nlabk&AN=512645

Selverston AI (1985) Model neural networks and behavior. Plenum Press, New York

Shaw KM, Park YM, Chiel HJ, Thomas PJ (2012) Phase resetting in an asymptotically phaseless system: On the phase response of limit cycles verging on a heteroclinic orbit. SIAM Journal on Applied Dynamical Systems 11:350–391, DOI 10.1137/110828976, URL http://link.aip.org/link/?SJA/11/350/1

Sherrington CS (1910) Flexion-reflex of the limb, crossed extension-reflex, and reflex stepping and standing. The Journal of Physiology 40(1-2):28–121, URL http://www.ncbi.nlm.nih.gov/pmc/articles/PMC1533734/

Sherwood WE, Guckenheimer J (2010) Dissecting the phase response of a model bursting neuron. SIAM Journal on Applied Dynamical Systems 9(3):659–703, DOI 10.1137/090773519, URL http://epubs.siam.org/doi/abs/10.1137/090773519

Shilnikov LP, Shilnikov AL, Turaev DV, Chua LO (2002) Methods of Qualitative Theory in Nonlinear Dynamics, Part II. World Scientific

Spardy LE, Markin SN, Shevtsova NA, Prilutsky BI, Rybak IA, Rubin JE (2011) A dynamical systems analysis of afferent control in a neuromechanical model of locomotion: II. phase asymmetry. Journal of Neural Engineering 8(6):065,004, DOI 10.1088/1741-2560/8/6/065004, URL http://iopscience.iop.org/1741-2560/8/6/065004

Stone E, Holmes P (1990) Random perturbations of heteroclinic attractors. SIAM Journal on Applied Mathematics 50(3):726–743, DOI 10.2307/2101884, URL http://www.jstor.org/stable/2101884

Susswein AJ, Chiel HJ (2012) Nitric oxide as a regulator of behavior: New ideas from *Aplysia* feeding. Progress in Neurobiology 97(3):304–317, DOI 10.1016/j.pneurobio.2012.03.004, URL http://www.sciencedirect.com/science/article/pii/S0301008212000366

Susswein AJ, Hurwitz I, Thorne R, Byrne JH, Baxter DA (2002) Mechanisms underlying fictive feeding in *Aplysia*: Coupling between a large neuron with plateau potentials activity and a spiking neuron. Journal of Neurophysiology 87(5):2307–2323, URL http://jn.physiology.org/content/87/5/2307.long

Sutton GP, Macknin JB, Gartman SS, Sunny GP, Beer RD, Crago PE, Neustadter DM, Chiel HJ (2004a) Passive hinge forces in the feeding apparatus of *Aplysia* aid retraction during biting but not during swallowing. Journal of Comparative Physiology A 190(6):501–514, DOI 10.1007/s00359-004-0517-4, URL http://link.springer.com/article/10.1007/s00359-004-0517-4

Sutton GP, Mangan EV, Neustadter DM, Beer RD, Crago PE, Chiel HJ (2004b) Neural control exploits changing mechanical advantage and context dependence to generate different feeding responses in *Aplysia*. Biological Cybernetics 91(5):333–345, DOI 10.1007/s00422-004-0517-z, URL http://link.springer.com/article/10.1007/s00422-004-0517-z

Tomori Z, Poliacek I, Jakus J, Widdicombe J, Donic V, Benacka R, Gresova S (2010) Distinct generators for aspiration and expiration reflexes: localization, mechanisms and effects. Journal of physiology and pharmacology: an official journal of the Polish Physiological Society 61(1):5–12

Vandorpe DH, Small DL, Dabrowski AR, Morris CE (1994) FMRFamide and membrane stretch as activators of the *Aplysia* S-channel. Biophysical Journal 66(1):46–58,

URL http://www.ncbi.nlm.nih.gov/pmc/articles/PMC1275662/

Varona P, Levi R, Arshavsky YI, Rabinovich MI, Selverston AI (2004) Competing sensory neurons and motor rhythm co-ordination. Neurocomputing 58-60:549–554, DOI 10.1016/j.neucom.2004.01.093, URL http://www.sciencedirect.com/science/article/B6V10-4BVP69M-M/2/c7aa0434cb0551bbe9ac6b1707b52ba7

Wallén P, Williams TL (1984) Fictive locomotion in the lamprey spinal cord in vitro compared with swimming in the intact and spinal animal. The Journal of Physiology 347(1):225–239, URL http://jp.physoc.org/content/347/1/225

White J, Rubinstein J, Kay A (2000) Channel noise in neurons. Trends Neurosci 23:131–137

Williams CD, Salcedo MK, Irving TC, Regnier M, Daniel TL (2013) The length–tension curve in muscle depends on lattice spacing. Proceedings of the Royal Society B: Biological Sciences 280(1766), DOI 10.1098/rspb.2013.0697, URL http://rspb.royalsocietypublishing.org/content/280/1766/20130697

Wilson DM (1961) The central nervous control of flight in a locust. Journal of Experimental Biology 38(2):471–490, URL http://jeb.biologists.org/content/38/2/471

Yu SN, Crago PE, Chiel HJ (1999) Biomechanical properties and a kinetic simulation model of the smooth muscle I2 in the buccal mass of *Aplysia*. Biological Cybernetics 81(5-6):505–13

Zajac FE (1989) Muscle and tendon: properties, models, scaling, and application to biomechanics and motor control. Critical reviews in biomedical engineering 17(4):359–411